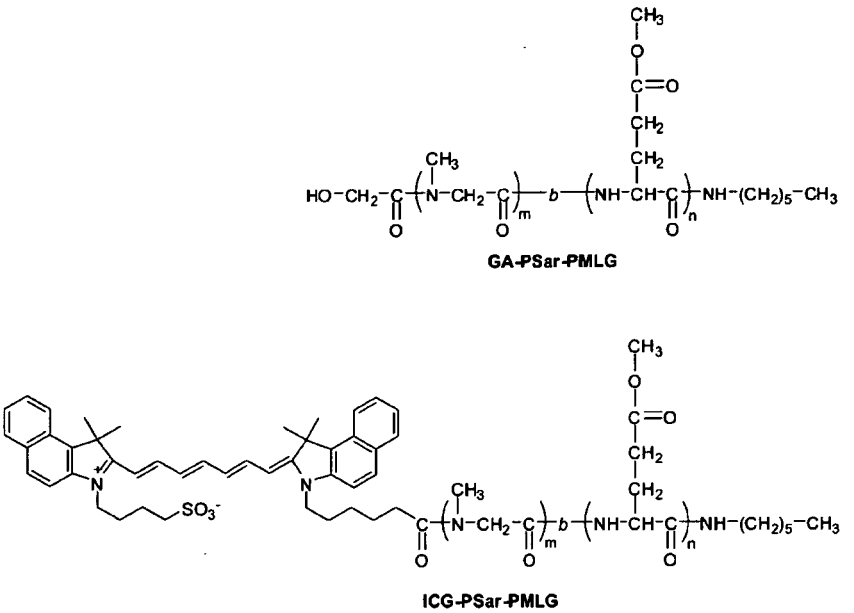

Figure 1. Chemical structures of amphiphilic block polypeptides, PSar-PMLGs. GA-PSar-PMLGs were used to prepare peptide assemblies, whereas ICG-PSar-PMLG was used for NIRF-labeling of peptosome.

is nonionic and hydrophilic like PEG, which will suppress the capture of the peptide assemblies by the RES due to the formation of a hydration layer on their surface (*42, 43*). Further, sarcosine is a naturally occurring amino acid, and the structure is a part of creatine which helps to supply energy to muscle cells. Sarcosine is degraded endogenously by sarcosine dehydrogenase. No side effect of sarcosine was reported except the cases of sarcosinaemia, and so forth (*44*). PSar is therefore expected to be biocompatible. PSar-PMLGs of a variety of compositions were synthesized via a sequential *N*-carboxyanhydride (NCA) polymerization method (*45*). NIRF-labeled peptosomes were successfully prepared with using PSar-PMLGs. *In vivo* experiments about retention in rat blood and NIRF imaging of cancer on mouse by using the peptosomes as nanocarrier are discussed.

EXPERIMENTAL PROCEDURES

Materials. All reagents and solvents were purchased commercially and were used as received unless otherwise noted. Solvents used for NCA preparation and polymerization and *n*-hexylamine used as an initiator were purified just before usage according to the ordinary procedures. ICG (indocyanine green)-Sulfo-OSu, DY-675, and m-dPEG12 amine were purchased from Dojin Laboratory Ltd., Dyomics GmbH, and Quanta BioDesign, Ltd., respectively, and was used as received.

Synthesis. Amphiphilic block polypeptides, PSar-PMLGs, were synthesized by the NCA polymerization method. PMLG block was obtained from γ-methyl-L-glutamate-*N*-carboxyanhydride (Glu(OMe)-NCA) using *n*-hexylamine as an initiator, followed by polymerization of sarcosine-*N*-carboxyanhydride (Sar-NCA). The number-average molecular weight of the polymers prepared in the present study was in the range 2800−8300. The *N*-terminal of the polypeptides was successively capped by glycolic acid using HATU as a coupling reagent to afford GA-PSar-PMLG, or by ICG-Sulfo-OSu to afford ICG-PSar-PMLG (Figure 1). Crude polypeptides were purified by a Sephadex LH20 column with *N,N*-dimethylformamide (DMF) as eluent. The compositions of the polypeptides were determined by ^{1}H NMR spectrum analysis using trifluoroacetic acid-*d* as deuterated solvent. Degrees of polymerization (DP) of PMLG and PSar blocks were determined from methyl ester protons and *N*-methyl protons, respectively, in comparison with signals from the initiator. The capping reaction of the *N*-terminal was also confirmed by ^{1}H NMR. The detail of the synthesis is as follows.

Sar-NCA. Benzyloxycarbonyl sarcosine (10.0 g, 44.8 mmol) was dissolved in $SOCl_2$ (10 mL), and the solution was shaken vigorously for 8 min at 50 °C. The solution was poured into petroleum ether (200 mL) to afford Sar-NCA as a white solid. The crude Sar-NCA was purified three times by recrystallization from ethyl acetate/petroleum ether. FT-IR: 1850, 1780 cm^{-1}. Melting point: 95–96 °C.

Glu(OMe)-NCA. To a suspension of H-Glu(OMe)-OH (7.11 g, 44.1 mmol) in tetrahydrofuran (THF, 70 mL) at 50 °C was added triphosgene (4.36 g, 14.7 mmol). After 1 h stirring, another triphosgene (0.86 g, 2.91 mmol) was added, and the mixture was stirred for 2 h. The reaction mixture was poured into hexane (210 mL), and the suspension was cooled at −20 °C to complete crystallization. The crude Glu(OMe)-NCA was purified two times by recrystallization from THF/hexane. FT-IR: 1850, 1780, 1710 cm^{-1}. Melting point: 95–97 °C.

GA-PSar-PMLG. To a solution of Glu(OMe)-NCA (0.1 M) in dry DMF under Ar atmosphere was added *n*-hexylamine with the amount of the specified monomer/initiator ratio in feed, and the solution was stirred for 3 h at room temperature. After confirmation of the disappearance of NCA signals from the solution by FT-IR measurement, Sar-NCA in DMF was added with the amount of the specified ratio of Sar block (PSar) and Glu(OMe) (PMLG) block in the copolymer. The solution was kept stirring until the NCA was fully consumed. To the solution were added glycolic acid (5 equiv), *O*-(7-azabenzotriazol-1-yl)-1,1,3,3-tetramethyluronium hexafluorophosphate (HATU) (5 equiv), and *N,N*-diisopropylethylamine (DIEA) (7.5 equiv) at 0 °C, and the solution was stirred at room temperature for 12 h under N_2 atmosphere. Additional portions of HATU (3 equiv) and DIEA (4 equiv) were added further to the solution at 0 °C, and the solution was kept stirring at room temperature for another 12 h under N_2 atmosphere. The solution was concentrated and purified by a Sephadex LH 20 column with DMF as eluent. The fraction of the copolymer was collected, and the product was precipitated from DMF/diethyl ether, followed by washing with acetone. The composition of PSar/PMLG in the

product was determined by ^{1}H NMR (trifluoroacetic acid (TFA)-*d*) with comparing the signal strengths of *N*-CH_3 of PSar, methyl ester of PMLG, and the terminal methyl of the initiator.

ICG-PSar-PMLG. Instead of glycol acid at the capping reaction in the preparation of GA-PSar-PMLG, ICG-sulfo-OSu (5 equiv of the terminal amino group) was added to the polymerization solution. The product was purified similarly to the case of GA-PSar-PMLG. The capping with ICG at the *N*-terminal of the copolymer was confirmed by ^{1}H NMR using 2,2,2-trifluoroethanol-d_3 as solvent.

DY-PEG. To a solution of DY-675 (5.0 mg, 7.1 μmol) and CH_3O-PEG_{12}-NH_2 (4.3 mg, 7.8 μmol, m-dPEG12 amine) in DMF were added HATU (3.0 mg, 7.8 μmol) and DIEA (2.0 μL, 12 μmol) at 0 °C, and the solution was stirred at room temperature for 6 h under N_2 atmosphere. HATU (0.55 mg, 1.4 μmol) and DIEA (0.37 μL, 2.6 μmol) were added further to the solution, and the solution was kept stirring at room temperature for another 16 h under N_2 atmosphere. The solution was concentrated under reduced pressure, and the residue was purified by a Sephadex LH 20 column with using DMF as eluent to afford the product. Mass analysis (FAB, matrix; nitrobenzylalcohol): *m/z* 1248.6 (calcd for $C_{67}H_{98}N_3O_{17}S$ $[(M + H)^+]$ *m/z* 1248.66).

Preparation of Aqueous Dispersion. Polypeptides were dispersed in a Tris-buffered saline (TBS) (10 mM Tris−HCl, 100 mM NaCl, pH 7.4) by the injection method using 2,2,2-trifluoroethanol (TFE) as solvent. GA-PSar-PMLG (4.5 mg) was dissolved in 75 μL of TFE, and the solution was rapidly injected into 1.5 mL of TBS, which was stirred and cooled on ice. The aqueous dispersion was applied on a Sephacryl S-100 column (1.5 × 30 cm, GE healthcare Bio-Sciences) using TBS as eluent to remove TFE and others. The peptide concentration was in the range 0.5–0.8 mg/mL. Labeling of the polypeptide assembly with NIRF was achieved by adding a few wt % of ICG-PSar-PMLG to GA-PSar-PMLG in a TFE solution before injection.

Dynamic Light Scattering Analysis. The size of the molecular assemblies formed in aqueous dispersion was analyzed by dynamic light scattering (DLS) on a Photal DLS-8000 (Otsuka Electronics Co., Japan) using a cylindrical optical cell of 1 cm diameter. Vertically polarized light of either wavelength 632.8 nm from a He−Ne laser or 488 nm from an Ar laser was used as the incident beam from a scattering angle of 90°. All measurements were performed at 25 °C. In order to avoid contamination of dust, all aqueous dispersions were prepared in a clean room and filtered through a 0.80 μm cellulose acetate membrane filter. The autocorrelation function was analyzed by the time interval method of photon correlation. The light scattering data were analyzed by the program of Contin (*46, 47*).

TEM Observation. TEM images were taken using a JEOL JEM-2000EXII at an accelerating voltage of 100 kV. For the observation of molecular assembly, a dispersion of GA-PSar56-PMLG12 in 10 mM Tris−HCl buffer (pH 7.4) was applied on a carbon-coated Cu grid, and the sample was stained negatively with 2% uranyl acetate, followed by suction of the excess fluid with a filter paper.

Encapsulation of Water-Soluble Drug Model. A solution of a mixture of GA-PSar43-PMLG18 and GA-PSar65-PMLG18 (3:1) and 1 wt % ICG-PSar63-PMLG20 in TFE was injected rapidly into 1.5 mL TBS containing 4 mg/mL FITC−dextran (MW: 4000). The mixture of ICG-labeled molecular assembly and FITC−dextran was applied on a Sephacryl S-100 column (1.5 × 30 cm) with using TBS as eluent, and the elution profile was monitored by absorbance at 780 and 490 nm of ICG and FITC, respectively. Encapsulation of DY-PEG was also done similarly to the method of encapsulation of FITC−dextran.

Circular Dichroism. To analyze the conformation of polypeptides in their aqueous dispersion, circular dichroism (CD) spectroscopy was carried out on a JASCO J600 spectropolarimeter with an optical cell of 0.1 cm optical path length at room temperature.

***In Vivo* Retention in Blood Measurement.** *In vivo* retention in blood of peptosome was evaluated by using rats as the experimental animals. Seven-week-old Crl:CD(SD) male rats were used. Peptosomes prepared from GA-PSar56-PMLG12 (n = 2) and a mixture of GA-PSar43-PMLG18 and GA-PSar65-PMLG18 (1:1) (n = 3) were NIRF-labeled with the addition of 5 wt % ICG-PSar63-PMLG20. The dispersions were administered at 0.8 mg/mL/kg to rats via tail vein. After administration of the peptosome, blood samples of 0.5 mL were taken temporally from rats and were centrifuged to collect the blood plasma samples. The amount of the ICG-labeled peptosome in the sample was estimated by fluorescence assay (Ex, 768 nm; Em, 807 nm). *In vivo* retention in the blood of the peptide micelle from GA-PSar93-PMLG12 and 5 wt % ICG-PSar63-PMLG20 was also evaluated by the same procedure (n = 2).

Cell Culture and Hypoxic Treatment *in Vitro*. SUIT-2 human pancreatic cancer cell line was purchased from the American type Culture Collection. SUIT-2/EF-Luc cells that carry the luciferase reporter gene under control of pEF constitutive promoter were isolated by the same method as described elsewhere. SUIT2/EF-Luc cells were maintained at 37 °C with 5% FBS-Dulbecco's modified Eagle medium (Nacalai Tesque, Kyoto, Japan).

Tumor Model. SUIT-2/pEF-luciferase cells were subcutaneously inoculated at 1 × 10^6 cells/mL of phosphate-buffered saline (PBS) into front legs, hind legs, or back of 8-week-old female nude mice (BALB/c nu/nu; Japan SLC Inc., Hamamatsu, Japan).

***In Vivo* Cancer Imaging.** For taking images of bioluminescence from the SUIT2/EF-luc xenografts, tumor-bearing mice were intraperitoneally injected with 100 μL D-luciferin solution (10 mg/mL in PBS; Promega Corp., Madison, WI). In 20 min, the mice were set in an IVIS-200 *in vivo* photon-counting device (Xenogen Corp., Alameda, CA). For taking fluorescence images from the NIRF-labeled peptosome, tumor-bearing mice were set in the IVIS-200 at the indicated time following intravenous injection of the peptosome dispersion (ca. 0.5 mg/mL, 200 μL). During imaging process, the mice were kept on the imaging stage under anesthetized condition with 2.5% of isoflurane gas in oxygen flow (1.5 L/min).

The fluorescence images from ICG were taken with the accessory ICG filter set, and those from DY-675 were taken with the Cy5.5/Cy5.5 Bkg filter sets. The pseudo images from the photon counts were constructed by *Living Image 2.50 - Igor Pro 4.09A* software (Xenogen Corp.).

RESULTS AND DISCUSSION

Synthesis of Polypeptides and Their Dispersibility in TBS. Amphiphilic block copolypeptides, GA-PSar-PMLGs and ICG-PSar-PMLG (Figure 1), were newly designed and synthesized by the conventional NCA method with the capping reaction using HATU as a coupling reagent or using active ester. Compositions of PSar-PMLGs were estimated by ^{1}H NMR analysis and found to be close to the monomer/initiator ratios in the feed (Table 1). GA-PSar-PMLGs having more than 43 sarcosine residues (entries 3–8) were dispersed stably in TBS by the TFE injection method (*48*), whereas those with shorter PSar chains yielded precipitates (entries 1, 2). Moderately long PSar chains are therefore necessary for PMLG chains of 12–18 residues to be dispersed stably in buffer.

Morphology of Molecular Assembly. Size and shape of molecular assembly of GA-PSar-PMLGs formed in buffer were analyzed by the DLS measurement and the TEM observation. Size distribution analysis by the DLS measurements suggested

Table 1. Compositions of PSar-PMLGs and Properties in Aqueous Dispersion

entry	monomer ratio in feed [Sar]/[Glu(OMe)]	composition of polypeptide [Sar]/[Glu(OMe)]	abbreviation[a]	molecular assembly[b]	size (nm)
1	15/15	15/12	GA-PSar15-PMLG12	precipitate (group PRE)	
2	25/15	25/12	GA-PSar25-PMLG12	precipitate (group PRE)	
3	40/20[e]	43/18	GA-PSar43-PMLG18	P (group PEP)	150
4	60/20	56/12	GA-PSar56-PMLG12	M, P (group MIC)	40, 150
5	60/20[e]	65/18	GA-PSar65-PMLG18	M, P (group MIC)	30, 90
6	80/20	93/12	GA-PSar93-PMLG12	M (group MIC)	40
7		entry 3/5=1/1[c]	mixture of GA-PSar43-PMLG18 and GA-PSar65-PMLG18 (1:1)	P, M (group PEP)	100, 30
8		entry 3/5=3/1[d]	mixture of GA-PSar43-PMLG18 and GA-PSar65-PMLG18 (3:1)	P, M (group PEP)	100, 30
9	60/20	63/20	ICG-PSar63-PMLG20		

[a] GA, capped *N*-terminal with glycolic acid, ICG, capped *N*-terminal with ICG-Sulfo-OSu. [b] P, peptosome, M, micelle, the former capital letter of P, M or M, P represents the predominant morphology of the mixed molecular assemblies. The block polypeptides are categorized into three groups, group PRE (precipitate), group PEP (peptosome), and group MIC (micelle), according to the predominant morphology in buffer (shown in the parentheses). [c] A mixture of GA-PSar43-PMLG18 and GA-PSar65-PMLG18 at the molar ratio of 1:1. [d] A mixture of GA-PSar43-PMLG18 and GA-PSar65-PMLG18 at the molar ratio of 3:1. [e] A solution of DMF and chloroform (3/1 v/v) was used for polymerization of entries 3 and 5. In other cases, DMF was used.

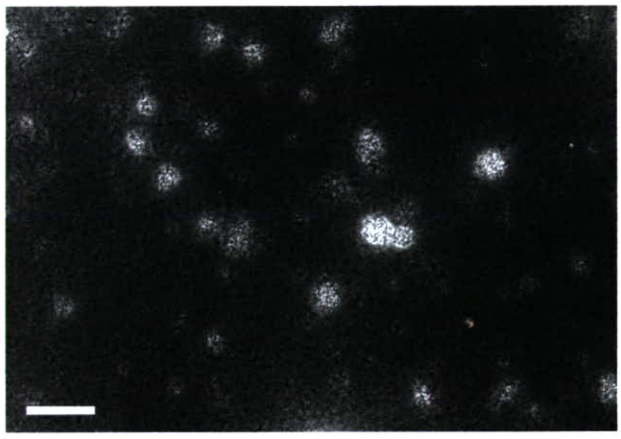

Figure 2. TEM image of peptosome in the aqueous dispersion of GA-PSar56-PMLG12. The sample was stained negatively with uranyl acetate. Scale bar represents 0.5 μm.

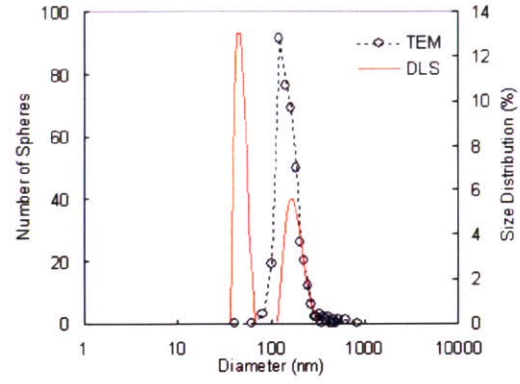

Figure 3. Comparison of size distributions determined by DLS measurement and TEM image (histogram). In both measurements, GA-PSar56-PMLG12 was used for preparation of the peptide assembly.

a bimodal distribution for some polypeptides (Table 1, entries 4, 5, 7, 8) due to formation of two types of molecular assemblies. However, the regularization procedure such as Contin used here may overfit the data to produce apparently two peaks. Indeed, upon changing the scattering angles in the DLS measurements, the bimodal distribution could become a smooth monomodal distribution in some cases. Table 1 shows two values as the molecular assembly size in some cases, but the sizes of the minor components are not thus fully convincing. In addition to the DLS measurements, we therefore analyzed the elution profiles of the molecular assemblies through gel permeation chromatography using Sephacryl S-100 or Sephadex 4B. The elution profiles were agreeable with the results of the DLS measurements summarized in Table 1. So, the sizes of the minor components of the molecular assemblies are shown in Table 1 despite their inaccuracy.

The fraction ratio of the two assemblies differs depending on the length of the PSar block in the copolypeptides. Diameter of the smaller assembly is in the range from 30 to 40 nm, and that of the larger one from 100 to 200 nm. Since the molecular length of GA-PSar-PMLGs is estimated to be about 20 nm with an extended form of the PSar block and α-helical conformation of the PMLG block, the smaller molecular assembly is assigned to a spherical micelle having a hydrophobic core and a hydrophilic shell.

An aqueous dispersion of GA-PSar56-PMLG12 was observed by TEM with negative staining (Figure 2). Spheres in the size range from 100 to 200 nm were present in the TEM image, and the size distribution of these large spheres is in agreement with that of the larger assemblies detected by DLS (Figure 3). Even though the detail analysis of the smaller assemblies detected by DLS was not possible by TEM due to the poor resolution, the peptide micelle should be formed with GA-PSar56-PMLG12 from the elution profile through gel permeation chromatography. On the other hand, GA-PSar43-PMLG18, a block polypeptide with a shorter PSar segment and a longer PMLG segment, formed the large spheres of ca. 150 nm from the DLS analysis (Table 1). These observations of amphiphilic polypeptides are consistent with previous reports that the morphology of molecular assemblies is related generally with the hydrophilic and hydrophobic balance of amphiphiles (*49, 50*); with increasing the hydrophobic property of amphiphiles, the major morphology shifts from a small micelle to cylinder and a large vesicle in water. When this relationship is applied to the present polypeptides, the large assembly of GA-PSar43-PMLG18 in buffer should be a vesicle. This structural point is discussed later with the encapsulation experiment.

Adjustment of the assembly size by mixing two kinds of polypeptides was examined (Table 1, entries 7, 8). Interestingly, the size of molecular assembly of GA-PSar43-PMLG18 was reduced from 150 to 100 nm by incorporation of GA-PSar65-PMLG18 at the molar ratios of 1:1 and 3:1 (GA-PSar43-PMLG18: GA-PSar65-PMLG18). The longer PSar block of GA-PSar65-PMLG18 in the mixture should favor staying at the outer surface of the spherical assembly to reduce the steric congestion compared with staying at the inner surface, resulting in a large curvature of the smaller spherical assembly. GA-PSar65-PMLG18 is thus considered to be inserted into the outer surface to increase the curvature of the vesicle due to the bulky PSar

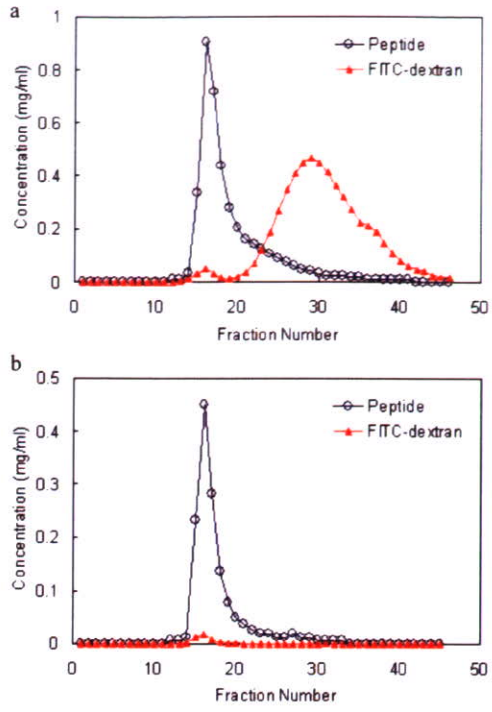

Figure 4. Encapsulation experiment of FITC−dextran in ICG-labeled molecular assembly prepared from a mixture of GA-PSar43-PMLG18 and GA-PSar65-PMLG18 (3:1). Elution profiles of size exclusion chromatography by a Sephacryl S-100 column were monitored by absorption of ICG (○) and fluorescein (▲). (a) First elution of the peptide dispersion prepared in a buffer containing FITC-dextran. (b) The repeated elution of the peptide fraction of the first elution.

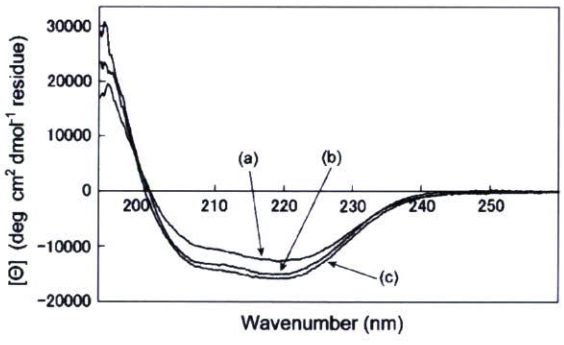

Figure 5. CD spectra of (a) GA-PSar43-PMLG18, (b) GA-PSar65-PMLG18, and (c) a mixture of GA-PSar43-PMLG18 and GAPSar65-PMLG18 (1:1) in 10 mM Tris buffer containing 0.1 M NaCl and 5% TFE. The residue concentration of Glu(OMe) was set at 5×10^{-4} M for all the samples.

block at the outer surface. The mixing effect on the assembly size, however, was not so sensitive in the mixing ratios of 1:1 and 3:1.

To obtain information on the molecular assembly of 100 nm, the encapsulation experiment was carried out with using the peptide assembly of a mixture of GA-PSar43-PMLG18 and GA-PSar65-PMLG18 (3:1) labeled with 1 wt % ICG-PSar63-PMLG20. The elution profile through a SEC column of the peptide assembly prepared in the presence of FITC-dextran (Mw: 4000) in buffer shows coelution of FITC−dextran with the peptide assembly (Figure 4a). The amount of the encapsulated dextran in the peptide assembly looks small, but the ratio of the encapsulated dextran against the total amount of dextran in buffer is consistent with the ratio of the total inner volume of the vesicles against the total solution

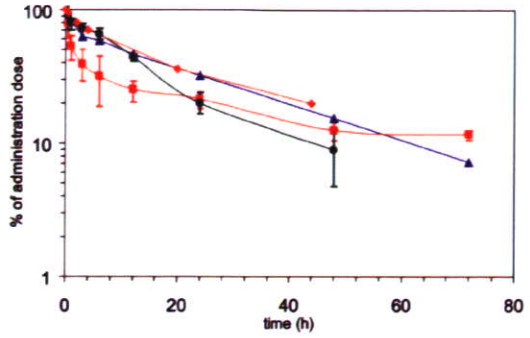

Figure 6. *In vivo* blood clearance curves of ICG-labeled peptosome (blue ▲, GA-PSar56-PMLG12; red ■, a mixture of GA-PSar43-PMLG18 and GA-PSar65-PMLG18 (1:1)) and ICG-labeled peptide micelle (green ●, GA-PSar93-PMLG12), in comparison with that of PEGylated liposomal doxorubicin, Doxil, in the literature (*53*) (orange ♦).

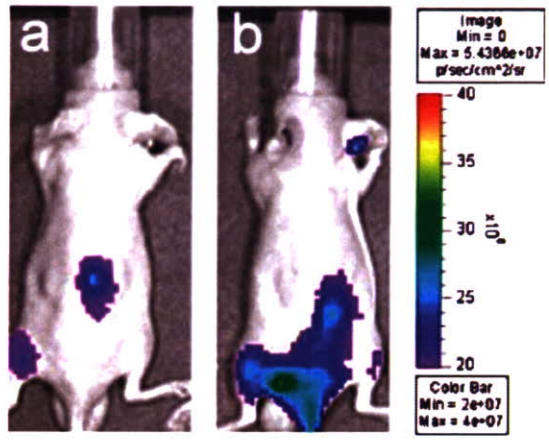

Figure 7. *In vivo* cancer imaging using NIRF-labeled peptosome. ICG-labeled peptosome prepared from a mixture of GA-PSar43-PMLG18 and GA-PSar65-PMLG18 (1:1) labeled with 3 wt % ICG-PSar63-PMLG20 was used. (a) Bioluminescence image of SUIT2/EF-luc xenografts on the tumor-bearing mouse after administration of D-luciferin. (b) Image of fluorescence from ICG, 1 day after the administration of ICG-labeled peptosome.

volume at the preparation, which was calculated under the following assumptions: the vesicular assembly of 100 nm diameter, the diameter of 2 nm for one peptide molecule occupying at the membrane, and interdigitation structure of the membrane. Further, the repeated column chromatography of the peptide fraction did not reduce the relative intensity of FITC−dextran, suggesting that FITC−dextran was encapsulated firmly in the vesicle (Figure 4b). Consequently, the peptide assembly of 100 nm has an inner aqueous phase to encapsulate a water-soluble compound, indicating the peptide assembly of vesicle, so-called "peptosome".

After our previous reports on preparation of peptosome in the size range of 100 nm (*39–41*), Deming et al. have also reported preparation of micrometer-sized vesicular assembly from ionic polypeptides (*51*). They reduced the size of assembly into about 100 nm by using the extruder method. In our case, a 100 nm sized peptosome was spontaneously formed only by injection of the peptide solution into buffer, and the size remained stable for weeks.

Conformation of polypeptides in the molecular assemblies was studied by CD spectroscopy. The aqueous dispersion of GA-PSar43-PMLG18 (group PEP; Table 1) showed negative Cotton effects at 222 and 208 nm (Figure 5), indicating α-helical conformation of the hydrophobic PMLG block (*52*). Since the signal at 222 nm was more intensive than that at 208 nm, α

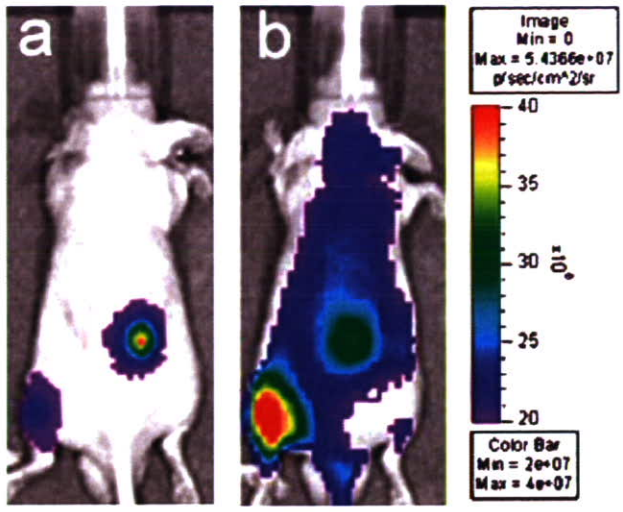

Figure 8. *In vivo* cancer imaging using NIRF-labeled peptide micelle. ICG-labeled peptide micelle prepared from GA-PSar93-PMLG12 labeled with 3 wt % ICG-PSar63-PMLG20 was used. (a) Bioluminescence image of SUIT2/EF-luc xenografts on the tumor-bearing mouse after administration of D-luciferin. (b) Image of fluorescence from ICG, 1 day after the administration of ICG-labeled peptide micelle.

helices should form a bundle structure in the peptide membrane. Similar results were obtained with GA-PSar65-PMLG18 (group MIC; Table 1) and a mixture of GA-PSar43-PMLG18 and GA-PSar65-PMLG18 (1:1) (group PEP). The α-helical structure in the peptide assembly makes a contrast to our previous report on amphiphilic poly(sarcosine)-*b*-poly(alanine), in which the hydrophobic poly(alanine) block took β-sheet structure in peptide micelle or aggregates (*27*). The conformation difference between these two types of block polypeptides in the molecular assemblies may be attributed to the difference of the side chains between alanine and Glu(OMe). The large hydrophobic side chain of Glu(OMe) may prevent the PMLG block from taking β-sheet structure of the tight molecular packing.

***In Vivo* Retention in Blood Measurement.** GA-PSar56-PMLG12 (group PEP) and a mixture of GA-PSar43-PMLG18 and GA-PSar65-PMLG18 (1:1) (group PEP) were chosen for preparation of about 100 nm sized peptosomes, and were subjected to *in vivo* retention in blood assay. The ICG-labeled peptosomes were administered to rats via a tail vein. Residual amounts of ICG-labeled peptosomes in blood plasma at different times were determined by fluorescence photometry (Figure 6). A small fraction of the peptosomes was cleared at the beginning stage, but the greatest part showed long retention circulating in the rat blood. When the two-compartment model was applied to the clearance curve, the half-lives at the β phase of the clearance curves were estimated to be about 20–40 h for these peptosomes. The relatively long half-life of the peptosomes is comparable to PEGylated liposome under the same experimental conditions (*54*).

ICG-labeled peptide micelle prepared from GA-PSar93-PMLG12 (group MIC) also showed a long retention circulation (Figure 6). However, the peptide micelle disappeared completely in 48 h, whereas a part of peptosome remained in blood even after 72 h from the injection. This result may be ascribed to the smaller size of the peptide micelle, which should promote its accumulation in liver (*55, 56*).

***In Vivo* Cancer Imaging.** *In vivo* NIRF imaging of cancer on mouse was carried out with using ICG-labeled peptosome prepared from a mixture of GA-PSar43-PMLG18 and GA-PSar65-PMLG18 (1:1) (group PEP). At 1 day after the administration, intensive fluorescence from ICG was observed at the two transplanted cancer sites (Figure 7b), which was confirmed by the bioluminescence from luciferin (Figure 7a). The peptosome is therefore considered to accumulate in the tumor tissue by the EPR effect.

ICG-labeled peptide micelle prepared from GA-PSar93-PMLG12 (group MIC) was also administered to the tumor-bearing mouse, and NIRF imaging was carried out. The intensive fluorescence from ICG was observed similarly at the tumor tissue (Figure 8). However, the fluorescence level at the background was moderately high. The peptide micelle may be

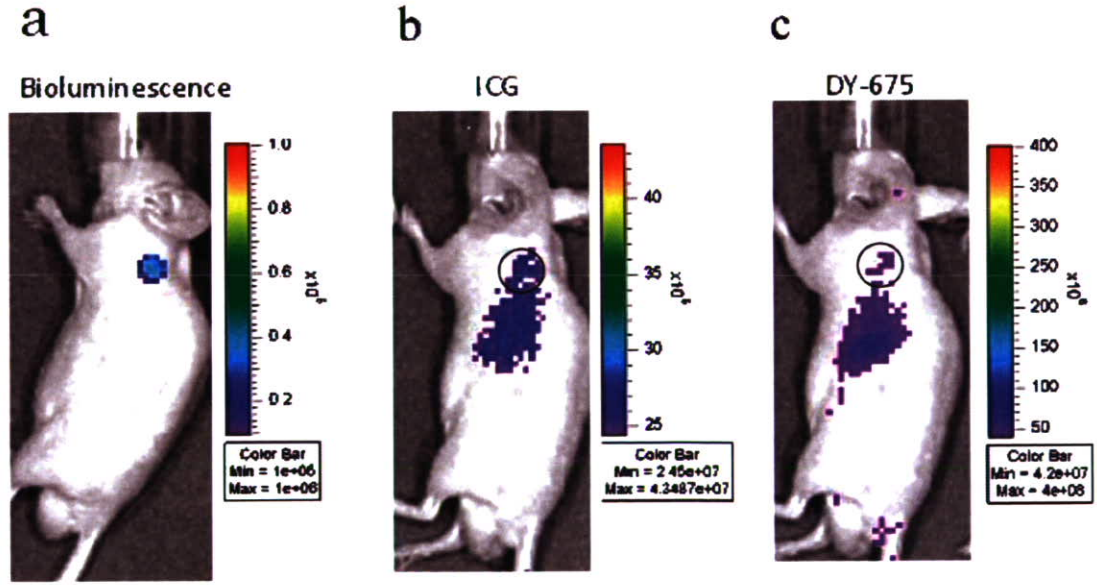

Figure 9. *In vivo* cancer imaging using NIRF-labeled peptosome encapsulating water-soluble far-red fluorophore. ICG-labeled peptosome prepared from a mixture of GA-PSar43-PMLG18 and GA-PSar65-PMLG18 (3:1) labeled with 3 wt % ICG-PSar63-PMLG20 and encapsulating DY-PEG in the inner aqueous phase (the concentration of DY-PEG was set at 4 mg/mL at the preparation). (a) Bioluminescence image of SUIT2/EF-luc xenografts on the tumor-bearing mouse after administration of D-luciferin. (b) Image of fluorescence from ICG, 2 days after the administration of peptosome. (c) Image of fluorescence from DY-675, 2 days after the administration of peptosome. Black circles in b and c represent the tumor site.

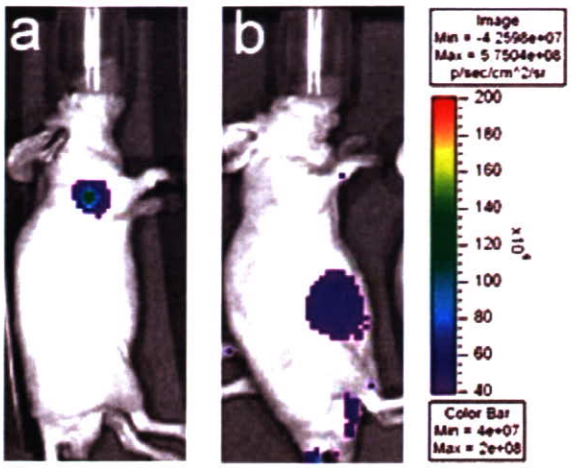

Figure 10. Control imaging experiment using water-soluble far-red fluorophore, DY-PEG. The amount of DY-PEG was adjusted to that used in the doubly labeled peptosome shown in Figure 9. (a) Bioluminescence image of SUIT2/EF-luc xenografts on the tumor-bearing mouse after administration of D-luciferin. (b) Image of fluorescence from DY-675, 2 days after the administration of DY-PEG.

partly incorporated into normal tissues probably due to the small size or physical instability.

Doubly labeled peptosome, in which the peptide membrane was labeled with ICG peptide and the inner aqueous phase encapsulated DY-675 labeled PEG (DY-PEG), was prepared and administered to the tumor-bearing mouse. These two kinds of fluorophores can be detected separately by choosing proper optical filters of the imaging apparatus, because ICG and DY-675 fluoresce at far-red and near-infrared region, respectively. ICG-labeled peptosome was prepared from a mixture of GA-PSar43-PMLG18 and GA-PSar65-PMLG18 (3:1) (group PEP) in a buffer containing DY-PEG. At 2 days after the intravenous administration to the tumor-bearing mouse, fluorescence from ICG was detected at the cancer site (Figure 9b), and at the same site, fluorescence from DY-675 was also observed (Figure 9c). In these images, accumulation of the peptosome in liver was also detected by both probes. On the other hand, when DY-PEG alone was administered to the tumor-bearing mouse, fluorescence at the cancer site was not observed at all even though accumulation in bladder was detected (Figure 10). Taken together, the peptosome was confirmed to be accumulated in the tumor tissue while maintaining its vesicular structure and preserving the water-soluble compound inside. The selective accumulation is therefore due to the EPR effect.

PSar chains around the peptosome are expected to take a role of suppressing the capture of peptosome by the RES, and *in vivo* retention in blood of peptosome was actually proven to be extremely long. In the case of PEGylated liposomes, the retention time in blood was improved by optimization of the mixing ratio of long and short PEG chains (*51*). Therefore, peptosome coated by optimized PSar layer may show further retention in blood, which is currently under investigation. Further, poly(ethylene glycol) (PEG), which is a common artificial water-soluble polymer and is used frequently for biocompatible materials, may be replaced with PSar in many cases.

In conclusion, we have succeeded in preparation of 100 nm sized peptosome, which is a vesicular assembly of genuine amphiphilic polypeptide, using PSar as a hydrophilic block and PMLG as a hydrophobic block. NIRF-labeled peptosome was prepared by adding ICG-conjugated polypeptide. Diameter of the peptosome prepared from GA-PSar-PMLGs was in the range from 100 to 200 nm, which is the appropriate size for the passive targeting into the solid tumor by the EPR effect. *In vivo* retention in blood of ICG-labeled peptosome was assayed by using rats as experimental animals, and the retention time was proven to be as long as the PEGylated liposome. ICG-labeled peptosome was also administered to the tumor-bearing mouse and successfully detected the tumor tissue due to the EPR effect.

ACKNOWLEDGMENT

This study is a part of joint research, which is focusing on the development of the basis of technology for establishing COE for nanomedicine, carried out through Kyoto City Collaboration of Regional Entities for Advancing Technology Excellence (CREATE) assigned by Japan Science and Technology Agency (JST). *In vivo* retention in blood studies were carried out with help of Termo Co. Japan.

LITERATURE CITED

(1) Weissleder, R., and Mahmood, U. (2001) Molecular imaging. *Radiology 219*, 316–333.

(2) Herschman, H. R. (2003) Molecular imaging: looking at problems, seeing solutions. *Science 302*, 605–608.

(3) Sharma, P., Brown, S., Walter, G., Santra, S., and Moudgil, B. (2006) Nanoparticles for bioimaging. *Adv. Colloid Interface Sci. 123*, 471–485.

(4) Tada, H., Higuchi, H., Watanabe, T. M., and Ohuchi, N. (2007) In vivo real-time tracking of single quantum dots conjugated with monoclonal anti-HER2 antibody in tumors of mice. *Cancer Res. 67*, 1138–1144.

(5) Josephson, L., Kircher, M. F., Mahmood, U., Tang, Y., and Weissleder, R. (2002) Near-infrared fluorescent nanoparticles as combines MR/optical imaginprobes. *Bioconjugate Chem. 13*, 554–560.

(6) Gao, X., Cui, Y., Levenson, R. M., Chung, L. W. K., and Nie, S. (2004) *In vivo* cancer targeting and imaging with semiconductor quantum dots. *Nat. Biotechnol. 22*, 969–976.

(7) Lyons, S. K. (2005) Advances in imaging mouse tumour models *in vivo*. *J. Pathol. 205*, 194–205.

(8) Ntziachristos, V., Bremer, C., and Weissleder, R. (2003) Fluorescence imaging with near-infrared light: new technological advances that enable in vivo molecular imaging. *Eur. Radiol. 13*, 195–208.

(9) HSu, A. R., Hou, L. C., Veeravau, A., Greve, J. M., Vogel, H., Tse, V., and Chen, X. (2006) *In vivo* near-infrared fluorescence imaging of integrin $\alpha_v\beta_3$ in an orthotopic glioblastoma model. *Mol. Imaging Biol. 8*, 315–323.

(10) Christian, N. A., Milone, M. C., Ranka, S. S., Li, G., Frail, P. R., Davis, K. P., Bates, F. S., Therien, M. J., Ghoroghchian, P. P., June, C. H., and Hammer, D. A. (2007) Tat-Functionalized near-infrared emissive polymersomes for dendritic cell labeling. *Bioconjugate Chem. 18*, 31–40.

(11) Cai, W., Shin, D.-W., Chen, K., Gheysens, O., Cao, Q., Wang, S. X., Gambhir, S. S., and Chen, X. (2006) Peptide-labeled near-infrared quantum dots for imaging tumor vasculature in living subjects. *Nano Lett. 6*, 669–676.

(12) Otsuji, E., Kuriu, Y., Okamoto, K., Ichikawa, D., Hagiwara, A., Ito, H., Nishimura, T., and Amagishi, H. (2006) Monoclonal antibody A7 coupled to magnetic particles as a contrast enhancing agent for magnetic resonance imaging of human colorectal carcinoma. *Cancer Immunol. Immunother. 55*, 728–733.

(13) Huh, Y.-M., Jun, Y.-W., Song, H.-T., Kim, S., Choi, J.-S., Lee, J.-H., Yoon, S., Kim, K.-S., Shin, J.-S., Suh, J.-S., and Cheon, J. (2005) *In vivo* magnetic resonance detection of cancer by using multifunctional magnetic nanocrystals. *J. Am. Chem. Soc. 127*, 12387–12391.

(14) Manchester, M., and Singh, P. (2006) Virus-based nanoparticles (VNPs): Platform technologies for diagnostic imaging. *Adv. Drug Delivery Rev. 58*, 1505–1522.
(15) Torchilin, V. P. (2007) Micellar nanocarriers: pharmaceutical perspectives. *Pharm. Res. 24*, 1–16.
(16) Lee, B.-S., Fujita, M., Khazenzon, N. M., Wawrowsky, K. A., Wachsmann-Hogiu, S., Farkas, D. L., Black, K. L., Ljubimova, J. Y., and Holler, E. (2006) Polycefin, a new prototype of a multifunctional nanoconjugate based on poly(L-malic acid) for drug delivery. *Bioconjugate Chem. 17*, 317–326.
(17) Matthews, S. E., Pouton, C. W., and Threadgill, M. D. (1996) Increased accumulation of PEG—PE micelles in the area of experimental myocardial infarction in rabbits. *Adv. Drug Delivery Rev. 18*, 219–267.
(18) Lukyanov, A. N., Hartner, W. C., and Torchilin, V. P. (2004) Increased accumulation of PEG—PE micelles in the area of experimental myocardial infarction in rabbits. *J. Controlled Release 94*, 187–193.
(19) Hashizume, H., Baluk, P., Morikawa, S., McLean, J. W., Thurston, G., Roberge, S., Jain, R. K., and McDonald, D. M. (2000) Openings between defective endothelial cells explain tumor vessel leakiness. *Am. J. Pathol. 156*, 1363–1380.
(20) Monsky, W. L., Fukumura, D., Gohongi, T., Ancukiewcz, M., Weich, H. A., Torchilin, V. P., Yuan, F., and Jain, R. K. (1999) Augmentation of transvascular transport of macromolecules and nanoparticles in tumors using vascular endothelial growth factor. *Cancer Res. 59*, 4129–4135.
(21) Turner, J. L., and Wooley, K. L. (2004) Nanoscale cage-like structures derived from polyisoprene-containing shell cross-linked nanoparticle templates. *Nano Lett. 4*, 683–688.
(22) Qi, K., Ma, Q., Remsen, E. E., Clark, C. G., Jr., and Wooley, K. L. (2004) Determination of the bioavailability of biotin conjugated onto shell cross-linked (SCK) nanoparticles. *J. Am. Chem. Soc. 126*, 6599–6607.
(23) Wang, F., Bronich, T. K., Kabanov, A. V., Rauh, R. D., and Roovers, J. (2005) Synthesis and evaluation of a star amphiphilic block copolymer from poly(ϵ-caprolactone) and poly(ethylene glycol) as a potential drug delivery carrier. *Bioconjugate Chem. 16*, 397–405.
(24) Discher, D. E., and Eisenberg, A. (2002) Polymer vesicles. *Science 297*, 967–973.
(25) Choucair, A., Lavigueur, C., and Eisenberg, A. (2004) Polystyrene-*b*-poly(acrylic acid) vesicle size control using solution properties and hydrophilic block length. *Langmuir 20*, 3894–3900.
(26) Schreief, H., and Bouwstrab, J. (1994) Liposomes and niosomes as topical drug carriers: dermal and transdermal drug delivery. *J. Controlled Release 30*, 1–15.
(27) Kidchob, T., Kimura, S., and Imanishi, Y. (1998) Amphiphilic poly(Ala)-b-poly(Sar) microspheres loaded with hydrophobic drug. *J. Controlled Release 51*, 241–248.
(28) Sengupta, S., Eavarone, D., Capila, I., Zhao, G., Watson, N., Kiziltepe, T., and Sasisekharan, R. (2005) Temporal targeting of tumour cells and neovasculature with a nanoscale delivery system. *Nature (London) 436*, 568–572.
(29) Koide, A., Kishimura, A., Osada, K., Jang, W.-D., Yamasaki, Y., and Kataoka, K. (2006) Semipermeable polymer vesicle (PICsome) self-assembled in aqueous medium from a pair of oppositely charged block. *J. Am. Chem. Soc. 128*, 5988–5989.
(30) Jaturanpinyo, M., Harada, A., Yuan, X., and Kataoka, K. (2004) Preparation of bionanoreactor based on core-shell structured polyion complex micelles entrappingtrypsin in the core cross-linked with glutaraldehyde. *Bioconjugate Chem. 15*, 344–348.
(31) Klibanov, A. L., Maruyama, K., Torchilin, V. P., and Huang, L. (1990) Amphipathic polyethyleneglycols effectively prolong the circulation time of liposomes. *FEBS Lett. 268*, 235–237.
(32) Papahadjopoulos, D., Allen, T. M., Gabizon, A., Mayhew, E., Matthay, K., Huang, S. K., Lee, K. D., Woodle, M. C., Lasic, D. D., Redemann, C., and Martin, F. J. (1991) Sterically stabilized liposomes: improvements in pharmacokinetics and antitumor therapeutic efficacy. *Proc. Natl. Acad. Sci. U.S.A. 88*, 11460–11464.
(33) Lyass, O., Uziely, B., Ben-Yosef, R., Tzemach, D., Heshing, N. I., Lotem, M., Brufman, G., and Gabizon, A. (2000) Correlation of toxicity with pharmacokinetics of pegylated liposomal doxorubicin (Doxil) in metastatic breast carcinoma. *Cancer 89*, 1037–1047.
(34) Muggia, F. M., Hainsworth, J. D., Jeffers, S., Miller, P., Groshen, S., Tan, M., Roman, L., Uziely, B., Muderspach, L., Garcia, A., Burnett, A., Greco, F. A., Morrow, C. P., Paradiso, L. J., and Liang, L. J. (1997) Phase II study of liposomal doxorubicin in refractory ovarian cancer: antitumor activity and toxicity modification by liposomal encapsulation. *J. Clin. Oncol. 15*, 987–993.
(35) Koukourakis, M. I., Koukouraki, S., Giatromanolaki, A., Archimandritis, S. C., Skarlatos, J., Beroukas, K., Bizakis, J. G., Retalis, G., Karkavitsas, N., and Helidonis, E. S. (1999) Liposomal doxorubicin and conventionally fractionated radiotherapy in the treatment of locally advanced non—small-cell Lung cancer and head and neck cancer. *J. Clin. Oncol. 17*, 3512–3521.
(36) Uziely, B., Jeffers, S., Isacson, R., Kutsch, K., Weitsao, D., Yehoshua, Z., Libson, E., Muggia, F. M., and Gabizon, A. (1995) Liposomal doxorubicin: antitumor activity and unique toxicities during two complementary phase I studies. *J. Clin. Oncol. 13*, 1777–1785.
(37) Obst, M., and Steinbüchel, A. (2004) Microbial degradation of poly(amino acid)s. *Biomacromolecules 5*, 1166–1176.
(38) Kidchob, T., Kimura, S., and Imanishi, Y. (1998) Thermoresponsive release from poly(Glu(OMe))-block-poly(Sar) microcapsules with surface-grafting of poly(N-isopropylacrylamide). *J. Controlled Release 50*, 205–214.
(39) Fujita, K., Kimura, S., and Imanishi, Y. (1999) Spherical self-assembly of a synthetic α-helical peptide in water. *Langmuir 15*, 4377–4379.
(40) Kimura, S., Kim, D. H., Sugiyama, J., and Imanishi, Y. (1999) Vesicular self-assembly of a helical peptide in water. *Langmuir 15*, 4461–4463.
(41) Kimura, S., Muraji, Y., Sugiyama, J., Fujita, K., and Imanishi, Y. (2000) Spontaneous vesicle formation by helical glycopeptides in water. *J. Colloid Interface Sci. 222*, 265–267.
(42) Osada, K., and Kataoka, K. (2006) Drug and gene delivery based on supramolecular assembly of PEG-Polypeptide hybrid block copolymers. *Adv. Polym. Sci. 202*, 113–153.
(43) Otsuka, H., Nagasaki, Y., and Kataoka, K. (2001) Self-assembly of poly(ethylene glycol)-based block copolymers for biomedical applications. *Curr. Opin. Colloid Interface Sci. 6*, 3–10.
(44) Tsai, G., Lane, H.-Y., Yang, P., Chong, M.-Y., and Lange, N. (2004) Glycine transporter I inhibitor, N-mehylglycine (sarcosine), added to antipsychotics for the treatment of Schizophernia. *Biol. Psychiatry 55*, 452–456.
(45) Kidchob, T., Kimura, S., and Imanishi, Y. (1996) Preparation, structure and release profile of polypeptide microcapsules. *J. Controlled Release 40*, 285–291.
(46) Provencher, S. W. (1988) A constrained regularization method for inverting data represented by linear algeraic or integral equations. *Comput. Phys. Commun. 27*, 213–227.
(47) Provencher, S. W. (1988) Contin: General purpose constrained regularization program for inverting noisy linear algeraic or integral equations. *Comput. Phys. Commun. 27*, 229–242.
(48) Pons, M., Foradada, M., and Estelrich, J. (1993) Liposomes obtained by the ethanol injection method. *Int. J. Pharm. 95*, 51–56.
(49) Cullis, P. R., and De Kruijiff, G. (1979) Lipid polymorphism and the functional roles of lipids in biological-membranes. *Biochim. Biophys. Acta 559*, 399–420.
(50) Van Hest, J. C. M., Delnoye, D. A. P., Baars, M. W. P. L., van Genderen, M. H. P., and Meijer, E. W. (1995) Polystyrene-

dendrimer apmphilic block-copolymers with a generation-dependent aggregation. *Science 268*, 1592–1595.

(51) Holowka, E. P., Pochan, D. J., and Deming, T. J. (2005) Charged polypeptide vesicles with controllable diameter. *J. Am. Chem. Soc. 127*, 12423–12428.

(52) Holzwarth, G., and Doty, P. (1965) The ultraviolet circular dichroism of polypeptides. *J. Am. Chem. Soc. 87*, 218–228.

(53) Bao, A. D., Goins, B., Klipper, R., Negrete, G., and Phillips, W. T. (2004) Direct ^{99m}Tc labeling of pegylated liposomal doxorubicin (Doxil) for pharmacokinetic and non-invasive imaging studies. *J. Pharmacol. Exp. Ther. 308*, 419–425.

(54) Klibanov, A. L., Maruyama, K., Beckerleg, A. M., Torchilin, V. P., and Huang, L. (1991) Activity of amphipathic poly(ethylene glycol) 5000 to prolong the circulation time of liposomes depends on the liposome size and is unfavorable for immunoliposome binding to target. *Biochim. Biophys. Acta 1062*, 142–148.

(55) Litzinger, D. C., Buiting, A. M. J., Vanrooijen, N., and Huang, L. (1994) Effect of liposome size on the circulation time and intraorgan distribution of amphipathic poly(ethylene glycol)-containing liposomes. *Biochim. Biophys. Acta 1190*, 99–107.

(56) Sadzuka, Y., Nakade, A., Tsuruda, T., and Sonobe, T. (2003) Study on the characterization of mixed polyethyleneglycol modified liposomes containing doxorubicin. *J. Controlled Release 91*, 271–280.

BC7001665

A EUROPEAN JOURNAL

CHEMBIOCHEM

OF CHEMICAL BIOLOGY

Table of Contents

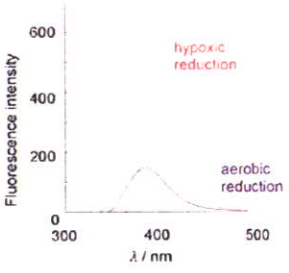

Hypoxia-imaging probes: A reactivity characteristic of indolequinone derivatives, substituents of which can be removed by one-electron reduction under anaerobic conditions, was exploited to develop a fluorescent probe for disease-relevant hypoxia. Only under hypoxic conditions does the conjugate IQ-Cou undergo decomposition to release a fluorescent coumarin chromophore upon X irradiation or incubation in the presence of a reduction enzyme (see graph).

WILEY-VCH

CHEMBIOCHEM

DOI: 10.1002/cbic.200700458

Emission under Hypoxia: One-Electron Reduction and Fluorescence Characteristics of an Indolequinone–Coumarin Conjugate

Kazuhito Tanabe,*[a] Nao Hirata,[a] Hiroshi Harada,[b, c] Masahiro Hiraoka,[b, c] and Sei-ichi Nishimoto*[a]

A characteristic feature of the reactivity of indolequinone derivatives, substituents of which can be removed by one-electron reduction under hypoxic conditions, was applied to the development of a new class of fluorescent probes for disease-relevant hypoxia. A reducing indolequinone parent molecule conjugated with fluorescent coumarin chromophores could suppress efficiently the fluorescence emission of the coumarin moieties by an intramolecular electron-transfer quenching mechanism and a conventional internal-filter effect. Under hypoxic conditions, however, the conjugate, denoted IQ-Cou, underwent a one-electron reduction triggered by X irradiation or the action of a reduction enzyme to release a fluorescent coumarin chromophore, whereupon an intense fluorescence emission with a maximum intensity at 420 nm was observed. The one-electron reduction of IQ-Cou was suppressed by molecular oxygen under aerobic conditions. IQ-Cou also showed intense fluorescence in a hypoxia-selective manner upon incubation with a cell lysate of the human fibrosarcoma cell line HT-1080. The IQ-Cou conjugate has several unique properties that are favorable for a fluorescent probe of hypoxia-specific imaging.

Introduction

Most cellular functions rely on the continuous and adequate supply of oxygen molecules from blood vessels. A stable oxygen supply is preserved in normal tissues by so-called oxygen homeostasis. An inadequate oxygen supply to cells induces hypoxia, which is one of the well-known pathophysiological characteristics of cardiac ischemia,[1] inflammatory diseases,[2] and solid tumors.[3] Tumor hypoxia is of particular importance, as it has been associated closely with the malignant phenotype of cancer cells, resistance to cancer therapies, and the low mortality rate of cancer patients.[3] Therefore, there has been increasing demand for hypoxia-specific molecular probes as useful indicators for the pathophysiological analysis of diseases.

We have developed prodrugs of the well-documented antitumor agents 5-fluorouracil (5-FU) and 5-fluorodeoxyuridine (5-FdUrd), which release 5-FU and 5-FdUrd, respectively, upon hypoxic X irradiation.[4] One 5-FdUrd prodrug with an indolequinone structure showed strong cytotoxicity against hypoxic tumor cells.[4a] Indolequinone derivatives have been identified by other research groups as a new class of hypoxia-specific prodrugs that can be activated to eliminate cytotoxic substituent components (active drugs) selectively by bioreduction or radiolytic reduction under hypoxic conditions.[5] These findings prompted us to investigate the development of hypoxia-imaging molecular probes containing a reducing indolequinone skeleton. Two coumarin chromophores were thus conjugated with an indolequinone unit through a 2,6-bis(hydroxymethyl)-*p*-cresol linker[6] to produce IQ-Cou, the indolequinone unit of which undergoes one-electron reduction to liberate three functional components through the spontaneous cyclization of a free-amine intermediate and the rearrangement of the resulting phenol derivative to the corresponding 1,4-quinone methide (Scheme 1). IQ-Cou itself showed weak fluorescence, because the fluorescent excited singlet state of the coumarin unit is quenched efficiently by the indolequinone unit located intramolecularly in close proximity. Upon the one-electron reduction of the indolequinone unit, the coumarin chromophore was eliminated and no longer affected by the fluorescence-quenching action of the indolequinone unit; thus, an intense fluorescence emission was observed. With these reaction characteristics, IQ-Cou might be applicable as a fluorescent probe for the molecular imaging of disease-relevant hypoxia.

Results and Discussion

The synthetic route to IQ-Cou is outlined in Scheme 2. The diol **3** was prepared by a previously described method[6] and cou-

[a] *Dr. K. Tanabe, N. Hirata, Prof. Dr. S.-i. Nishimoto*
Department of Energy and Hydrocarbon Chemistry
Graduate School of Engineering, Kyoto University
Katsura Campus, Nishikyo-ku, Kyoto 615-8510 (Japan)
Fax: (+81) 75-383-2504
E-mail: tanabeka@scl.kyoto-u.ac.jp
nishimoto@scl.kyoto-u.ac.jp

[b] *Dr. H. Harada, Prof. M.D. M. Hiraoka*
Department of Radiation Oncology and Image-Applied Therapy
Graduate School of Medicine, Kyoto University
Shogoin, Sakyo-ku, Kyoto 606-8507 (Japan)

[c] *Dr. H. Harada, Prof. M.D. M. Hiraoka*
Nano-Medicine Merger Education Unit, Kyoto University
Shogoin, Sakyo-ku, Kyoto 606-8507 (Japan)

Supporting information for this article is available on the WWW under http://www.chembiochem.org or from the author.

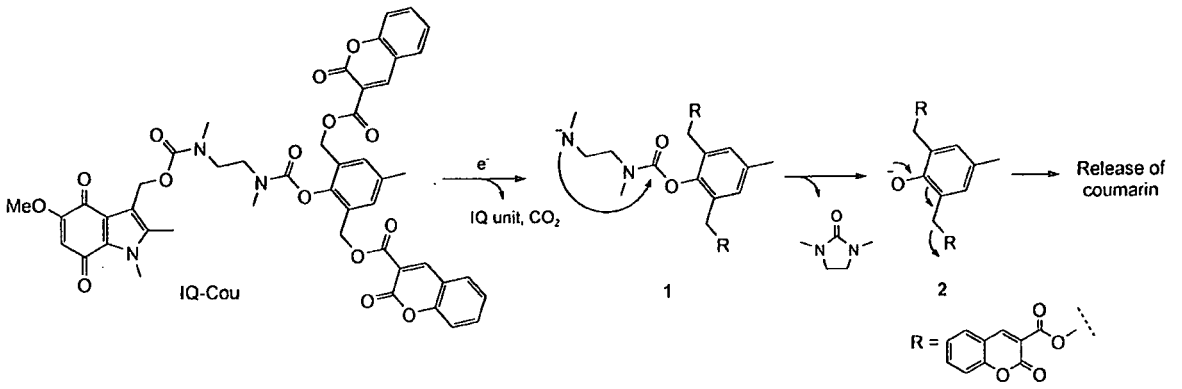

Scheme 1. Mechanism for the activation of IQ-Cou to release a fluorescent coumarin chromophore under reductive conditions.

pled with the acid chloride **8** to form **4**. The diester **4** was converted into the free amine under acidic conditions and then coupled with the indolequinone derivative **7** (prepared from the alcohol **6**[7]) to give IQ-Cou.

We first compared the fluorescence spectrum of IQ-Cou with that of the reference compound coumarin-3-carboxylic acid (Figure 1 A). Whereas coumarin-3-carboxylic acid showed an intense fluorescence emission at about 420 nm upon excitation at a wavelength of 300 nm, the apparent fluorescence intensity of IQ-Cou was extremely weak: The formal fluorescence quantum yields (Φ_f) of coumarin-3-carboxylic acid and IQ-Cou were 0.042 and 0.002, respectively. These results indicate that the fluorescence of the coumarin chromophore in IQ-Cou is quenched intramolecularly by the neighboring indolequinone unit and predict that fluorescence emission will be restored upon the one-electron reduction of IQ-Cou to release a coumarin-3-carboxylic acid fragment.

The suppressed fluorescence emission of IQ-Cou is attributable to two modes of action of the indolequinone unit. First, a conventional internal filter effect due to the presence of the indolequinone unit could lead to a decrease in the apparent fluorescence quantum yield of the counterpart coumarin chromophore by about a third in view of the similarity of the molar extinction coefficients at 300 nm of coumarin-3-carboxylic acid and the indolequinone **6** ($\varepsilon = 6206$ and $5863\ M^{-1}cm^{-1}$, respectively).[8] Second, a photoinduced electron-transfer (PET) process[9] should be operative as a key mechanism for modulating the fluorescence properties of IQ-Cou. The PET that leads to fluorescence quenching can occur between the excited states of an electron-withdrawing (electron-donating) fluorophore

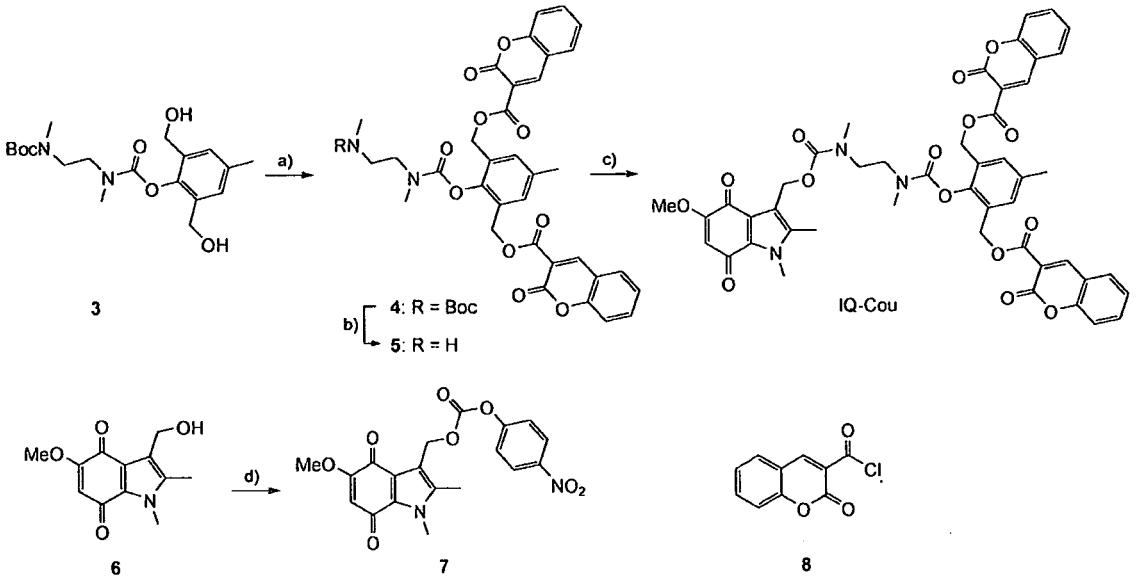

Scheme 2. Reagents and conditions: a) **8**, Et_3N, CH_2Cl_2, room temperature, 62%; b) HCl, MeOH, room temperature; c) **7**, Et_3N, CH_2Cl_2, room temperature, 39% (two steps); d) 4-nitrophenyl chloroformate, Et_3N, CH_2Cl_2, 0 °C, 37%. Boc = *tert*-butoxycarbonyl.

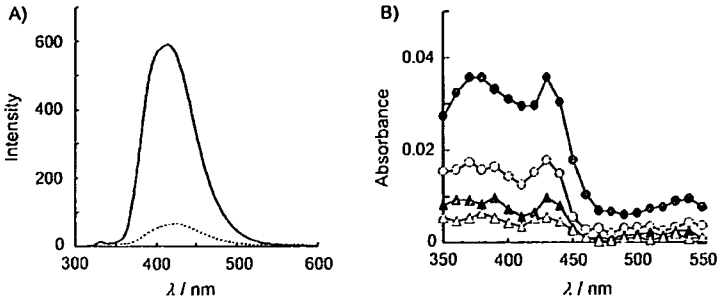

Figure 1. A) Fluorescence spectra of IQ-Cou (10 μM; ——) and coumarin-3-carboxylic acid (10 μM; ····) in acetonitrile. The fluorescence spectra were measured with excitation at 300 nm. B) Transient absorption spectra observed upon the excitation at 355 nm of IQ-Cou (30 μM) in acetonitrile; 1 (●), 10 (○), 20 (▲), and 30 μs (△) after laser flash photolysis.

and an electron-donating (electron-withdrawing) quencher. The feasibility of the process depends on the relative ordering of the energy levels of the highest occupied molecular orbitals (HOMO) and the lowest unoccupied molecular orbitals (LUMO) of the fluorophore and the quencher.[10] The MO energy levels of 3-methoxycarbonylcoumarin and the indolequinone **6** were estimated by ab initio calculations at the B3LYP/6-31G(d) level, which revealed that the LUMO energy level of **6** (−2.94 eV) is lower than that of coumarin (−2.25 eV), whereas the HOMO energy level of **6** (−6.15 eV) is higher than that of coumarin (−6.77 eV). These calculation results suggest strongly that an intramolecular electron transfer from coumarin in the excited state to the indolequinone unit in the ground state is feasible thermodynamically in IQ-Cou.

We also carried out laser flash photolysis studies to gain further insight into the suppressed fluorescence emission of IQ-Cou. Figure 1B shows the transient absorption spectra observed in the laser flash photolysis at 355 nm of IQ-Cou in acetonitrile. The transient absorption appeared 1 μs after the laser flash. An absorption in the region 360–390 nm was assigned to the semiquinone radical anion.[4a,5d] We also observed a transient absorption at 410–440 nm that may be assigned to the coumarin radical cation.[11] This absorption decayed in a similar way to that of the semiquinone radical anion. These results indicate that the photolysis of IQ-Cou induces electron transfer from the excited coumarin unit to the indolequinone unit. Thus, we concluded that indolequinone could suppress efficiently the fluorescence emission of coumarin by an intramolecular electron-transfer mechanism.

We measured the changes in the fluorescence spectrum of IQ-Cou upon X irradiation. An argon-purged, aqueous solution of IQ-Cou in the presence of excess 2-methylpropan-2-ol was used for these experiments. Under these conditions, IQ-Cou undergoes one-electron reduction, whereby the indolequinone unit, with a lower LUMO energy level, may capture reducing hydrated electrons (e_{aq}^-) generated as a primary intermediate of water radiolysis.[12,13] As shown representatively in Figure 2, the intensity of the fluorescence at about 420 nm assigned to coumarin-3-carboxylic acid increased with increasing irradiation dose upon hypoxic X irradiation of IQ-Cou. The fluorescence after 720 Gy of X irradiation was three times as intense as that of IQ-Cou in the absence of irradiation (Figure 2A). These results indicate clearly that IQ-Cou is activated to release coumarin-3-carboxylic acid from the indolequinone quencher by radiolytic one-electron reduction by e_{aq}^- with the restoration of fluorescence.

A smaller enhancement in fluorescence emission occurred upon aerobic irradiation: The sample solution showed only a 1.5-fold increase in fluorescence intensity upon exposure to 720 Gy of X irradiation (Figure 2B). This oxygen effect on the activation of

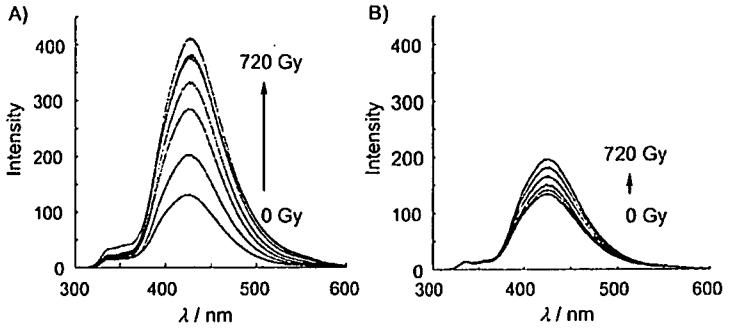

Figure 2. Changes in the fluorescence spectrum of IQ-Cou upon X irradiation. IQ-Cou (100 μM) was irradiated, and then the fluorescence spectra were measured with excitation at 300 nm. A) Fluorescence spectra observed after hypoxic irradiation of IQ-Cou (from bottom to top: 0, 72, 144, 288, 528, 720 Gy). B) Fluorescence spectra observed after aerobic irradiation of IQ-Cou (from bottom to top: 0, 72, 144, 288, 528, 720 Gy).

IQ-Cou can be accounted for by the reactivity of molecular oxygen, which captures efficiently reducing e_{aq}^- species to form a superoxide anion radical ($O_2^{\cdot-}$). Furthermore, recent studies on the reductive activation of indolequinone prodrugs suggest that a semiquinone anion radical intermediate generated by the one-electron reduction of the indolequinone unit could reduce molecular oxygen to form the original indolequinone and $O_2^{\cdot-}$, a process that would lead to a decrease in the net yield of the released drug.[4a] Because of the reaction characteristics of molecular oxygen, the described radiolytic activation of IQ-Cou to enhance the fluorescence emission is likely to occur substantially under hypoxic conditions.

We also monitored the course of the radiolytic reduction of IQ-Cou and release of coumarin-3-carboxylic acid with time by a reversed-phase HPLC (Figure 3). Upon the hypoxic X irradiation of an argon-purged, aqueous solution of IQ-Cou in the presence of excess 2-methylpropan-2-ol, the concentrations of decomposed IQ-Cou and released coumarin-3-carboxylic acid increased with increasing radiation dose. *G* values[13] of 218.9 and 15.2 nmol J^{-1} were found for the decomposition of IQ-Cou and the release of coumarin, respectively.[14] Consistent with the smaller change in fluorescence intensity in the aerobic irradiation of IQ-Cou, the decomposition of IQ-Cou was suppressed to a *G* value of 16.5 nmol J^{-1} and the release of cou-

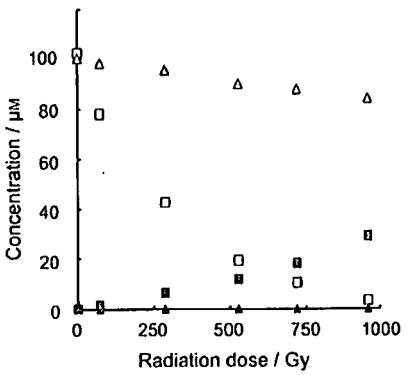

Figure 3. X-Radiolysis (4.0 Gy min^{-1}) of IQ-Cou (100 μM; open symbols) in aqueous solution containing 30% 2-methylpropan-2-ol at ambient temperature under hypoxic (square) and aerobic (triangle) conditions, with the release of coumarin-3-carboxylic acid (filled symbols).

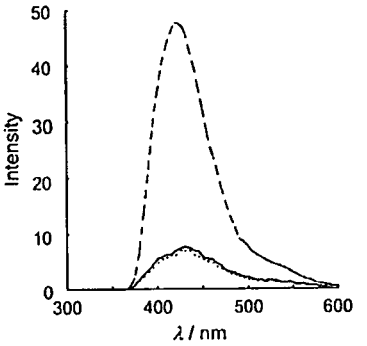

Figure 4. Fluorescence spectra of IQ-Cou after treatment with reductase. IQ-Cou (500 μM) was incubated with NADPH:cytochrome P450 reductase (10.6 μg mL^{-1}) and β-NADPH (2 mM) at 37 °C for 45 min at three different oxygen concentrations (< 0.5 mg L^{-1}: ----; 8.2 mg mL^{-1}: ——; > 20 mg mL^{-1}: ....).[16] The fluorescence spectra were measured with excitation at 300 nm.

marin-3-carboxylic acid was not detected under aerobic conditions. Thus, the concentration change of coumarin-3-carboxylic acid upon irradiation correlates well with the change in fluorescence intensity.

To characterize the biological one-electron reduction of IQ-Cou, we subjected IQ-Cou to enzymatic reduction. NADPH:cytochrome P450 reductase is an electron-donating protein that catalyzes the one-electron reduction of quinone derivatives to semiquinone anion radicals. Evidence that NADPH:cytochrome P450 reductase is expressed in many pathological tissues[15] stimulated us to carry out the bioreduction of IQ-Cou. We incubated IQ-Cou with NADPH:cytochrome P450 reductase and the cofactor β-NADPH at three different oxygen concentrations (<0.5, 8.2, and >20 mg L^{-1}). An intense fluorescence emission was observed for the solution of IQ-Cou incubated with <0.5 mg L^{-1} oxygen as a model of hypoxia (Figure 4). At an oxygen concentration of 8.2 mg L^{-1}, as under aerobic conditions, the extent of enhanced fluorescence intensity diminished significantly as a result of the competitive scavenging by molecular oxygen of hydrated electrons, e_{aq}^-, and the semiquinone radical to inhibit partially the reductive fragmentation of IQ-Cou. Thus, IQ-Cou was activated by NADPH:cytochrome P450 reductase in a hypoxia-selective manner, in accord with the results of radiolytic reduction. We also confirmed the hypoxia-selective release of coumarin-3-carboxylic acid from IQ-Cou upon treatment with NADPH:cytochrome P450 reductase, as monitored by HPLC (see the Supporting Information).

To further assess the function of IQ-Cou, we studied the reaction of IQ-Cou upon treatment with a cell lysate. IQ-Cou was incubated at 37 °C for 4 h under hypoxic and aerobic conditions with a lysate of the human fibrosarcoma cell line HT-1080. After incubation, the samples were filtered and analyzed by fluorescence spectrophotometry and HPLC. An intense fluorescence emission at about 420 nm was observed for the sample incubated under hypoxic conditions (Figure 5A). The intensity of the emission was four times as strong as that of the sample incubated under aerobic conditions. The difference in the fluorescence intensity of the two samples correlates well with the corresponding yields of coumarin-3-carboxylic acid from IQ-Cou, as quantified independently by HPLC (Figure 5B). We also confirmed that the incubation of IQ-Cou in a buffer solution resulted in a similar fluorescence intensity to that observed for the sample incubated aerobically. These results indicate strongly that IQ-Cou undergoes one-electron reduction by intracellular reductase to release fluorescent coumarin-3-carboxylic acid under hypoxic conditions.

In this study, we developed a new type of hypoxia-specific fluorescence imaging probe. IQ-Cou is activated efficiently by intracellular reductase under hypoxic conditions. Although low expression of NADPH:cytochrome P450 reductase was reported for the HT-1080 cell line,[17] an intense fluorescence emission was observed for IQ-Cou even upon treatment with HT-1080 cell lysate under hypoxic conditions. IQ-Cou may therefore be expected to show more intense fluorescence emission when incorporated in certain hypoxic tumor cells with higher reductase expression. In view of the hypoxia-specific fluorescence emission of IQ-Cou, the one-electron reduction of indolequinone derivatives could be a promising strategy for the detection of disease-relevant hypoxia. However, IQ-Cou has some drawbacks: First, an inner-filter effect due to the overlapping of the absorption of indolequinone with that of coumarin leads to the apparent suppression of fluorescence emission. Therefore, fluorescent molecules that absorb in a wavelength region that does not coincide with the absorption of indolequinone should be employed to establish a highly sensitive hypoxia-specific fluorescence imaging probe. Second, the fluorescence spectrum of coumarin-3-carboxylic acid occurs at around 420 nm, that is, at wavelengths that are too short to be applied to the imaging of deep-seated malignant tissues. One of the key strategies for in vivo optical imaging is the employment of near-infrared (NIR) light, because hemoglobin, as a principle absorber of visible light, and water and lipids, as principle absorbers of infrared light, have their lowest absorption in the NIR region, at around 650–900 nm.[18] Moreover, tissue autofluorescence observed in the NIR region has a minimum intensity. From this point of view, it is essential to apply dyes with fluorescence at NIR wavelengths to the present strategy with indolequinone derivatives.

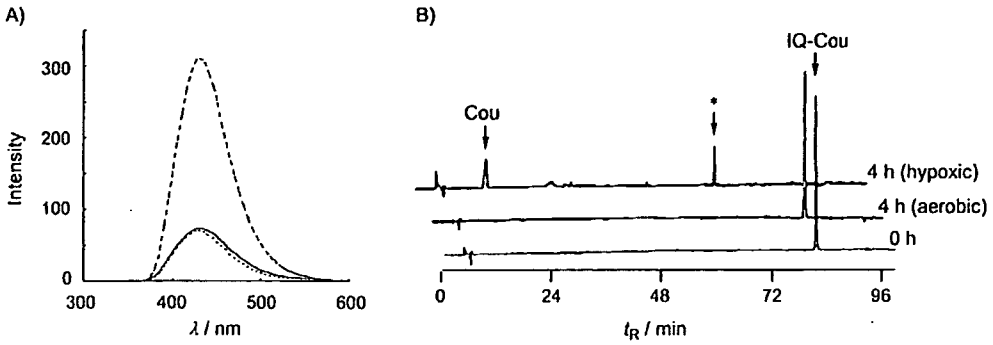

Figure 5. Treatment of IQ-Cou with a cell lysate obtained from the human fibrosarcoma cell line HT-1080. IQ-Cou (500 μM) was incubated with the cell lysate for 4 h at 37 °C under hypoxic or aerobic conditions. A) The fluorescence spectra[16] of IQ-Cou upon treatment with the cell lysate under hypoxic (·····) or aerobic conditions (——). IQ-Cou was also incubated alone in a buffer solution as a control (····). The fluorescence spectra were measured with excitation at 300 nm. B) HPLC profiles of IQ-Cou (500 μM) upon treatment with the cell lysate for 0 and 4 h under hypoxic or aerobic conditions. The HPLC signal indicated "Cou" was identified as coumarin-3-carboxylic acid. The HPLC signal indicated with the symbol "*" possibly corresponds to a reaction intermediate; however, the compound could not be identified because of its low stability and prompt degradation.

Conclusions

In summary, we have characterized the reactivity by one-electron reduction of IQ-Cou, which was synthesized as a hypoxia-specific fluorescence probe. IQ-Cou consists of a hypoxia-sensitive oxidizing indolequinone parent unit, two fluorescent coumarin chromophores, and a 2,6-bis(hydroxymethyl)-*p*-cresol linker. Both radiolytic and enzymatic one-electron reduction under hypoxic conditions lead to the efficient decomposition of IQ-Cou, with the release of coumarin-3-carboxylic acid accompanied by intense fluorescence. A similar enhancement in fluorescence emission was also observed in a hypoxia-selective manner upon the incubation of IQ-Cou with an HT-1080 cell lysate. Thus, it appears that IQ-Cou can be activated by intracellular reductase. Although IQ-Cou is a promising candidate as a hypoxia-specific fluorescence imaging tool, the absorption and emission of the coumarin fluorophore at relatively short wavelengths is a disadvantage. Furthermore, it is necessary to characterize the reactivity of the probe with potentially reactive species in living cells in detail to establish a molecular system for hypoxia imaging. Our current studies focus on the construction of a hypoxia-specific imaging probe that is sensitive to NIR light and thereby applicable to in vivo optical imaging.

Experimental Section

General methods: NMR spectra were recorded on a 270-MHz JMN-AL-270 (JEOL), 300-MHz JMN-AL-300 (JOEL), or 400-MHz JMN-AL-400 (JOEL) spectrophotometer at ambient temperature. Chemical shifts are reported in ppm relative to the residual solvent peak. Mass spectra were recorded on a JMS-SX102 A (JOEL) mass spectrometer, with a glycerol or *m*-nitrobenzylalcohol (NBA) matrix as an internal standard. All reactions were carried out under a dry nitrogen atmosphere with freshly distilled solvents, unless otherwise noted. Reagents were purchased from Aldrich, Wako Pure Chemical Industries, or Nacalai Tesque and used without purification. NADPH:cytochrome P450 reductase and β-NADPH coenzyme were obtained from Oxford Biomedical Research and Oriental Yeast Co., respectively. Tetrahydrofuran was distilled under a nitrogen atmosphere from sodium/benzophenone ketyl immediately prior to use. Ultrapure water was obtained from a Yamato WR-600 A water purifier. Precoated TLC (Merck silica gel 60 F_{254}) plates were used for monitoring the reactions. Wako gel (C-300, Wako Pure Chemical Industries) was used for column chromatography. A Rigaku Radioflex-350 X-ray generator was employed for X radiolysis at ambient temperature. High-performance liquid chromatography (HPLC) was carried out with a Shimadzu HPLC system (SPD-10A UV/Vis detector, CT0-10A column oven, two LC-10AS pumps, C-R6A chromatopac). Sample solutions were injected onto a reversed-phase column (Inertsil ODS-3, GL Science Inc., ø 4.6×150 nm). The following solvent program was used: of 88.9% B (20 min) followed by 88.9–16.7% B (a linear gradient over 70 min; solution A: 95% acetonitrile; solution B: 5% acetonitrile containing 0.1 M triethylammonium acetate (TEAA) buffer, pH 5). Fluorescence spectra were recorded with excitation at 300 nm on a Shimadzu RF-5300PC spectrofluorophotometer at ambient temperature, whereby a UV-33 glass filter (Toshiba Glass Co.) was set on the detector side to cut off the excitation peak at 300 nm. The amount of dissolved oxygen (DO) was measured with an OM-51 DO meter (Horiba) at 37 °C. Compound **7** was prepared from compound **6** as reported elsewhere.[7] The human fibrosarcoma cell line, HT-1080, was purchased from American Type Culture Collection (Manassas, VA) and maintained in Dulbecco Modified Eagle Medium (Invitrogen) containing fetal bovine serum (10%) in a humidified incubator with 5% CO_2, 95% air at 37 °C.

Preparation of compound 4: Coumarin-3-carboxylic acid (510 mg, 2.68 mmol) was dissolved in thionyl chloride (5 mL), and the resulting mixture was stirred at 100 °C for 2.5 h. The mixture was then concentrated by evaporation to give the acid chloride **8**, which was used immediately, without purification, in the next step.

The crude acid chloride **8** was added as a solution in dichloromethane (2 mL) and Et_3N (1 mL) to a solution of **3** (254 mg, 0.66 mmol) in dichloromethane (3 mL), and the resulting mixture was stirred at 0 °C for 15 min, and then at ambient temperature for 3 h. The reaction mixture was then diluted with saturated aqueous sodium hydrogen carbonate and extracted with chloroform. The organic layer was washed with brine, dried over anhydrous magnesium sulfate, filtered, and concentrated in vacuo. The crude product was purified by flash chromatography (SiO_2, 33% hexane/ethyl acetate) to give **4** (300 mg, 62%) as a brown oil. ^1H NMR (300 MHz, $CDCl_3$; as a result of restricted rotation about the amide bond adja-

cent to the linker, two signals were observed for some atoms): $\delta =$ 8.49 and 8.46 (s, 2H), 7.57–7.49 (m, 4H), 7.29–7.17 (m, 6H), 5.22 (s, 4H), 3.54–3.23 (m, 4H), 3.08, 2.83, and 2.67 (s, 6H), 2.28 (s, 3H), 1.32 and 1.29 ppm (s, 9H); ^{13}C NMR (68 MHz, $CDCl_3$; as a result of restricted rotation about the amide bond adjacent to the linker, two signals were observed for some atoms): $\delta = 162.0$, 156.3, 154.9, 154.0, 149.0, 148.9, 145.9, 136.0, 135.9, 134.3, 131.7, 131.4, 129.5, 128.4, 124.7, 117.6, 117.4, 117.3, 116.5, 79.6, 62.6, 62.5, 47.5, 47.1, 46.3, 35.5, 35.3, 34.9, 29.6, 28.4, 20.9, 14.2 ppm; FABMS (NBA/$CHCl_3$): *m/z* 727 $[M+H]^+$; HRMS: *m/z* calcd for $C_{39}H_{39}N_2O_{12}$: 727.2498 $[M+H]^+$; found: 727.2505.

Preparation of IQ-Cou: Compound **4** (155 mg, 0.21 mmol) was added to 0.5 M HCl/MeOH (2 mL), and the mixture was stirred for 14 h at ambient temperature. The solvent was then removed under reduced pressure to give **5** (181 mg) as a colorless oil. The crude product **5** was dissolved in *N,N*-dimethylformamide (DMF; 1 mL).

The indolequinone derivative **7** (177 mg, 0.44 mmol) in DMF (1 mL) was added to the solution of **5** in DMF, and the resulting mixture was stirred at ambient temperature for 8 h. The mixture was then diluted with saturated aqueous sodium hydrogen carbonate and extracted with ethyl acetate. The organic layer was washed with brine, dried over anhydrous magnesium sulfate, filtered, and concentrated in vacuo. The crude product was purified by flash chromatography (SiO_2, from 16.7% ethyl acetate/hexane to 100% ethyl acetate) to give IQ-Cou (72.1 mg, 39%) as an orange oil. ^{1}H NMR (300 MHz, $CDCl_3$, room temperature; as a result of restricted rotation about the amide bonds, two signals were observed for some atoms): $\delta = 8.55$ and 8.51 (s, 2H), 7.58–7.53 (m, 4H), 7.31–7.20 (m, 6H), 5.52–5.39 (m, 1H), 5.24–5.04 (m, 6H), 3.83–3.66 (m, 6H), 3.58–2.74 (m, 10H), 2.31 (s, 3H), 2.24 and 2.19 ppm (s, 3H); ^{1}H NMR (400 MHz, [D$_6$]DMSO, 120 °C): $\delta = 8.62$ (s, 2H), 7.83 (d, $J = 0.02$ Hz, 2H), 7.72 (t, $J = 0.02$ Hz, 2H), 7.38 (t, $J = 0.02$ Hz, 6H), 5.61 (s, 1H), 5.27–5.13 (br, 4H), 5.11 (s, 2H), 3.74 (s, 3H), 3.71 (s, 3H), 3.48–3.33 (m, 5H), 2.92–2.69 (m, 5H), 2.36 (s, 3H), 2.19 ppm (s, 3H); ^{13}C NMR (100 MHz, $CDCl_3$, room temperature; as a result of restricted rotation about the amide bonds, two signals were observed for some atoms): $\delta = 178.4$, 177.0, 162.1, 159.3, 156.4, 155.0, 154.1, 149.3, 149.0, 145.7, 138.1, 136.0, 134.3, 131.4, 129.6, 129.0, 128.5, 124.7, 121.6, 117.77, 117.75, 117.3, 116.6, 106.5, 62.5, 57.5, 56.3, 47.2, 46.7, 35.7, 35.3, 35.0, 32.3, 21.0, 9.6, 9.4 ppm; ^{13}C NMR (100 MHz, [D$_6$]DMSO, 120 °C): $\delta = 177.3$, 176.3, 163.0, 161.5, 158.9, 155.1, 154.2, 152.8, 147.8, 145.1, 137,5, 134.6, 133.8, 129.8, 129.5, 128.3, 127.8, 124.2, 120.6, 117.2, 117.1, 115.6, 115.1, 106.2, 61.4, 56.7, 55.8, 46.3, 45.8, 34.2, 33.9, 31.3, 19.8, 8.3 ppm; FABMS (NBA/$CHCl_3$): *m/z* 888 $[M+H]^+$; HRMS: *m/z* calcd for $C_{47}H_{42}N_3O_{15}$: 888.2610 $[M+H]^+$; found: 888.2604.

Measurement of extinction coefficients: The extinction coefficients (ε) of compound **6** and coumarin-3-carboxylic acid were calculated according to the Beer–Lambert law. UV spectra of the samples in acetonitrile (final concentration: 120 μM) were recorded with a Jasco V-530 UV/Vis spectrometer.

Fluorescence spectrophotometry: Fluorescence spectra of IQ-Cou and coumarin-3-carboxylic acid in acetonitrile (final concentration: 10 μM) were recorded with a Shimadzu RF-5300PC fluorescence spectrophotometer with excitation at 300 nm.

Measurement of fluorescence quantum yield: The fluorescence quantum yield (Φ_F) was determined by using Coumarin 153, with a known Φ_F value of 0.42 in methanol, as a reference. The area of the emission spectrum was integrated by using instrumentation software, and the quantum yield was calculated according to Equation (1), in which $\Phi_{F(S)}$ and $\Phi_{F(R)}$ are the fluorescence quantum yields of the sample and the reference, respectively, the terms $A_{(S)}$ and $A_{(R)}$ refer to the area under the fluorescence spectra, $(Abs)_{(R)}$ and $(Abs)_{(S)}$ are the optical densities of the sample and reference solutions at the excitation wavelength, and $n_{(S)}$ and $n_{(R)}$ are the refractive indices of the solvents used for the sample and the reference.

$$\Phi_{F(S)}/\Phi_{F(R)} = \frac{A_{(S)}}{A_{(R)}} \frac{(Abs)_{(R)}}{(Abs)_{(S)}} \frac{n_{(S)}^2}{n_{(R)}^2} \quad (1)$$

Laser flash photolysis: Laser flash photolysis was carried out with a Unisoku TSP-601 flash spectrometer. A continuum Surelite-I Nd-YAG (Q-switched) laser with the fourth harmonic at 355 nm was employed for flash photoirradiation. The probe beam from a Hamamatsu 150-W xenon short-arc lamp was guided with an optical fiber scope to a perpendicular orientation with respect to the excitation laser beam. The probe beam was monitored with a Unisoku MD200 photomultiplier tube through a Hamamatsu DG535 image-intensifier controller (1024 photodiodes). The timing of the excitation pulse laser, the probe beam, and the detection system was achieved through a Tektronix model TDS 3012 digital phosphor oscilloscope interfaced to an IBM Windows XP computer. A solution of IQ-Cou (30 μM) in acetonitrile was deaerated by bubbling argon through it prior to laser flash photolysis.

Radiolytic reduction: To establish hypoxia, an aqueous solution of IQ-Cou (100 μM) containing 2-methyl-2-propanol (30%) was purged with argon for 30 min and then irradiated in a sealed glass ampoule at ambient temperature with an X-ray source (4.0 Gy min^{-1}). After irradiation, aliquots were taken at appropriate time intervals for fluorescence spectrophotometry, and then diluted by 33% with Milli-Q water for analytical HPLC. A control air-saturated sample solution was irradiated and analyzed in a similar manner.

Bioreduction by NADPH–P450 reductase: To establish hypoxia, a solution of NADPH:cytochrome P450 reductase (final concentration: 10.6 μg mL^{-1}) and β-NADPH (final concentration: 2 mM) in phosphate buffer (25 mM, pH 7.4) was purged with argon for 10 min at 37 °C. IQ-Cou (final concentration: 500 μM) was added to the resulting solution, which was then incubated at 37 °C. For analytical HPLC, aliquots were taken at appropriate time intervals and diluted by 10% with Milli-Q water/acetonitrile (1:1). The reaction mixture was extracted with ethyl acetate to remove β-NADPH coenzyme, and florescence spectra of the organic layer were measured with excitation at 300 nm. A control aerobic sample solution was irradiated and analyzed in a similar manner.

Bioreductive activation of IQ-Cou by HT-1080 cell lysate: HT-1080 cells were cultured in six dishes (90% confluent in dishes of 100 mm in diameter) and washed twice with ice-cold phosphate-buffered saline. The cell lysate was then harvested with ice-cold CelLytic M cell lysis reagent (2 mL; Sigma–Aldrich), maintained at ambient temperature for 15 min, and centrifuged at 14000 rpm for 5 min to remove the cell debris. The resulting supernatant was kept in a Bactron II anaerobic environmental chamber (Sheldon Manufacturing, Cornelius, OR; 94% N_2, 5% CO_2, 1% H_2) at 37 °C for 22 h for hypoxic treatment. IQ-Cou (final concentration: 500 μM) was added to the hypoxic lysate, which was then incubated at 37 °C for 4 h. Aliquots were taken at appropriate time intervals, diluted by 10% with a 1:1 mixture of Milli-Q water and acetonitrile, and then diluted by 50% with acetonitrile. All solutions were filtered with a Cosmonice Filter S (Nacalai Tesque, Kyoto, Japan) for analytical HPLC and fluorescence spectrophotometry. Normoxic

lysate, which was kept in a well-oxygenated incubator (95% air, 5% CO_2, 37 °C), and lysis buffer alone were mixed in a similar way with IQ-Cou and analyzed as negative controls.

Acknowledgements

This study is part of joint research focused on the development of a basis of technology for establishing COE of nanomedicine, carried out through the Kyoto City Collaboration of Regional Entities for Advancing Technology Excellence (CREATE) assigned by the Japan Science and Technology Agency (JST).

Keywords: enzymes · fluorescent probes · hypoxia · indolequinones · one-electron reduction

[1] a) G. L. Semenza, *Annu. Rev. Med.* **2003**, *54*, 17–28; b) G. L. Semenza, *Trends Mol. Med.* **2001**, *7*, 345–350; c) G. L. Semenza, *Pediatr. Res.* **2001**, *49*, 614–617.

[2] C. Murdoch, M. Muthana, C. E. Lewis, *J. Immunol.* **2005**, *175*, 6257–6263.

[3] a) S. Kizaka-Kondoh, M. Inoue, H. Harada, M. Hiraoka, *Cancer Sci.* **2003**, *94*, 1021–1028; b) A. L. Harris, *Nat. Rev. Cancer* **2002**, *2*, 38–47.

[4] a) K. Tanabe, Y. Makimura, Y. Tachi, A. Imagawa-Sato, S. Nishimoto, *Bioorg. Med. Chem. Lett.* **2005**, *15*, 2321–2324; b) Y. Shibamoto, Y. Tachi, K. Tanabe, H. Hatta, S. Nishimoto, *Int. J. Radiat. Oncol. Biol. Phys.* **2004**, *58*, 397–402; c) K. Tanabe, Y. Mimasu, A. Eto, Y. Tachi, S. Sakakibara, M. Mori, H. Hatta, S.-i. Nishimoto, *Bioorg. Med. Chem.* **2003**, *11*, 4551–4556; d) Y. Shibamoto, L. Zhou, H. Hatta, M. Mori, S. Nishimoto, *Int. J. Radiat. Oncol. Biol. Phys.* **2001**, *49*, 407–413; e) M. Mori, H. Hatta, S. Nishimoto, *J. Org. Chem.* **2000**, *65*, 4641–4647; f) Y. Shibamoto, L. Zhou, H. Hatta, M. Mori, S.-i. Nishimoto, *Jpn. J. Cancer Res.* **2000**, *91*, 433–438.

[5] a) M. Hernick, C. Flader, R. F. Borch, *J. Med. Chem.* **2002**, *45*, 3540–3548; b) S. A. Everett, E. Swann, M. A. Naylor, M. R. L. Stratford, K. B. Patel, A. Tian, R. G. Newman, B. Vojnovic, C. J. Moody, P. Wardman, *Biochem. Pharmacol.* **2002**, *63*, 1629–1639; c) E. Swann, P. Barraja, A. M. Oberlander, W. T. Gardipee, A. R. Hundnott, H. D. Beall, C. J. Moody, *J. Med. Chem.* **2001**, *44*, 3311–3319; d) M. A. Naylor, E. Swann, S. A. Everett, M. Jaffar, J. Nolan, N. Robertson, S. D. Lockyer, K. B. Patel, M. F. Dennis, M. R. L. Stratford, P. Wardman, G. E. Adams, C. J. Moody, I. J. Stratford, *J. Med. Chem.* **1998**, *41*, 2720–2731.

[6] M. Shamis, H. N. Lode, D. Shabat, *J. Am. Chem. Soc.* **2004**, *126*, 1726–1731.

[7] Z. Zhang, K. Tanabe, H. Hatta, S. Nishimoto, *Org. Biomol. Chem.* **2005**, *3*, 1905–1910.

[8] As two coumarin chromophores are conjugated with an indolequinone unit in IQ-Cou, the indolequinone unit could absorb about $^1/_3$ of the total incident UV light at 300 nm to suppress the apparent fluorescence quantum yield of the counterpart coumarin chromophore to about $^2/_3$ of the intrinsic quantum yield in the absence of an indolequinone unit.

[9] a) T. Ueno, Y. Urano, K. Setsukinai, H. Takakusa, H. Kojima, K. Kikuchi, K. Ohkubo, S. Fukuzumi, T. Nagano, *J. Am. Chem. Soc.* **2004**, *126*, 14079–14085; b) T. Miura, Y. Urano, K. Tanaka, T. Nagano, K. Ohkubo, S. Fukuzumi, *J. Am. Chem. Soc.* **2003**, *125*, 8666–8671; c) K. Tanaka, T. Miura, N. Umezawa, Y. Urano, K. Kikuchi, T. Higuchi, T. Nagano, *J. Am. Chem. Soc.* **2001**, *123*, 2530–2536.

[10] G. J. Kavarnos, *Fundamentals of Photoinduced Electron Transfer*; VCH, Weinheim, **1993**.

[11] The transient signals of the radical cations of coumarin derivatives were reported to appear at 390–450 nm; see: a) L. Chen, P. D. Wood, A. Mnyusiwalla, J. Marlinga, L. J. Johnston, *J. Phys. Chem. B* **2001**, *105*, 10927–10935; b) P. D. Wood, L. J. Johnston, *J. Phys. Chem. A* **1998**, *102*, 5585–5591; c) K. I. Priyadarsini, D. B. Naik, P. N. Moorthy, *Chem. Phys. Lett.* **1988**, *148*, 572–576.

[12] Radiolysis of a dilute aqueous solution at about pH 7.0 produces primary water radicals, such as oxidizing hydroxyl radicals ('OH), reducing hydrated electrons (e^-_{aq}), and reducing hydrogen atoms ('H) with the *G* values (see ref. [10]) 2.8×10^{-7}, 2.8×10^{-7}, and 0.6×10^{-7} mol J^{-1}, respectively. In the presence of excess 2-methylpropan-2-ol, oxidizing 'OH is scavenged, and reduction proceeds almost exclusively.

[13] The *G* value is defined as the number of moles produced or changed per 1 J of radiation energy absorbed by the reaction system.

[14] Hydrated electrons were reported to show high reactivity toward carbonyl groups: a) E. J. Hart, E. M. Fielden, M. Anbar, *J. Phys. Chem.* **1967**, *71*, 3993–3998; b) W. M. Garrison, *Chem. Rev.* **1987**, *87*, 381–398 This side reaction may be one of the reasons for the low yield of free coumarin upon hypoxic X irradiation.

[15] L. J. Yu, J. Matis, D. A. Scudiero, K. M. Hite, A. Monk, E. A. Sausville, D. J. Waxman, *Drug Metab. Dispos.* **2001**, *29*, 304–312.

[16] The fluorescence emission of coumarin-3-carboxylic acid was influenced by the pH variation. Fluorescence quantum yield of this fluorophore at pH 3.6, 7.4 and 11.8 were 0.012, 0.0016 and 0.0015, respectively. To avoid the pH effect on the fluorescence spectra, we measured fluorescence of the sample after extraction or dilution by organic solvents. (see Experimental Section).

[17] R. L. Cowen, K. J. Williams, E. C. Chinje, M. Jaffar, F. C. D. Sheppard, B. A. Telfer, N. S. Wind, I. J. Stratford, *Cancer Res.* **2004**, *64*, 1396–1402.

[18] R. Weissleder, V. Ntziachristos, *Nat. Med.* **2003**, *9*, 123–128.

Received: August 7, 2007
Published online on January 25, 2008

Oncogene (2007) 26, 7508–7516

www.nature.com/onc

ORIGINAL ARTICLE

Significance of HIF-1-active cells in angiogenesis and radioresistance

H Harada[1,2], S Kizaka-Kondoh[1,3], G Li[1,5], S Itasaka[1], K Shibuya[1], M Inoue[4] and M Hiraoka[1]

[1]*Department of Radiation Oncology and Image-Applied Therapy, Kyoto University Graduate School of Medicine, Kyoto, Japan;* [2]*Nano-Medicine Merger Education Unit, Kyoto University, Kyoto, Japan;* [3]*COE Formation for Genomic Analysis of Disease Model Animals with Multiple Genetic Alterations, Kyoto University Graduate School of Medicine, Kyoto, Japan and* [4]*Department of Biochemistry, Osaka Medical Center for Cancer and Cardiovascular Diseases, Osaka, Japan*

Human solid tumors contain hypoxic regions that have considerably lower oxygen tension than the normal tissues. Hypoxia offers resistance to radiotherapy and anticancer chemotherapy, as well as predispose to increased tumor metastases. Furthermore, hypoxia induces hypoxia-inducible factor-1 (HIF-1), which in turn increases tumor angiogenesis. Thus, eradication of HIF-1-active/hypoxic tumor cells is very important for cancer therapy. We have previously reported that procaspase-3 fused with a von Hippel–Lindau (VHL)-mediated protein destruction motif of alpha subunit of HIF-1 (HIF-1α) containing Pro564, named TAT-ODD-procaspase-3 (TOP3), specifically induced cell death to hypoxic cells *in vivo* as well as *in vitro*. We now report that TOP3 also eradicates the radiation-induced HIF-1-active tumor cells. HIF-1 activity in the xenografts of human tumor cells, which express luciferase under the transcriptional control of HIF-1, were monitored and quantified daily with an *in vivo* bioluminescence photon-counting device. HIF-1 activity in tumors was more rapidly increased by ionizing radiation (IR) compared to untreated tumors. TOP3 efficiently decreased the HIF-1-activity in irradiated tumors as well as unirradiated ones, indicating TOP3 eradicated tumor cells with HIF-1-activity induced by IR as well as hypoxia. Eradication of HIF-1-active/hypoxic cells in the xenografts during irradiation exhibited significant suppression in angiogenesis and strong enhancement in a long-term growth suppression of tumor xenografts. These results further strengthen the argument that HIF-1-active/hypoxic cells play crucial roles in angiogenesis and radioresistance.

Oncogene (2007) **26**, 7508–7516; doi:10.1038/sj.onc.1210556; published online 11 June 2007

Keywords: tumor hypoxia; angiogenesis; HIF-1; radiotherapy

Correspondence: Dr S Kizaka-Kondoh, Department of Radiation Oncology and Image-applied Therapy, Kyoto University Graduate School of Medicine, 54 Kawahara-cho, Shogoin, Sakyo-ku, Kyoto 606-8507, Japan.
E-mail: skondoh@kuhp.kyoto-u.ac.jp
[5]Current address: Cancer Center, The General Hospital of Chinese People's Armed Police Forces, Yongding Road 69, Haidian District, Beijing 100039, China.
Received 7 March 2007; revised 18 April 2007; accepted 25 April 2007; published online 11 June 2007

Introduction

Reduced oxygen tension far below physiological levels is a characteristic of solid tumors (Vaupel *et al.*, 1989; Harris, 2002; Brown and Wilson, 2004). Polarographic needle electrode analysis and immunohistochemical analysis with antibodies against hypoxia markers have demonstrated that solid tumors contain severely hypoxic regions, in which pO_2 values are less than 10 mmHg (Höckel *et al.*, 1993; Raleigh *et al.*, 1998). Because oxygen has the highest affinity for electrons among any molecule in the cell, it reacts rapidly with unpaired electrons of free radicals in irradiated DNA, thereby aggravating radiation damage (Brown, 1999; Vaupel, 2001). Therefore, cytocidal effects of ionizing radiation (IR) are severely compromised under low oxygen tension, making hypoxia a critical limitation for the success of radiotherapy.

Hypoxia-inducible factor-1 (HIF-1) is expressed in hypoxic tumor cells. In addition, HIF-1 is also induced transiently in tumors following radiotherapy in response to the reoxygenation stress, and this induction peaked at around 48 h after irradiation (Moeller *et al.*, 2004). HIF-1 transactivates various hypoxia-responsive genes, which confer malignant properties to tumors such as apoptosis resistance, enhanced tumor growth, invasion and metastasis (Semenza, 2003). In addition, HIF-1 activates proangiogenic cytokines such as vascular endothelial growth factor (VEGF) and platelet-derived growth factor, which confer radiation resistance to endothelial cells as well as increase the proliferation and regrowth of tumor blood vessels (Gorski *et al.*, 1999; Geng *et al.*, 2001; Abdollahi *et al.*, 2003; Moeller *et al.*, 2004). Neovascularization is a particularly important contribution of HIF-1 to the survival and regrowth of tumors after irradiation (Abdollahi *et al.*, 2003). Thus, hypoxia impacts tumor radioresponsiveness not only in altering the physicochemical properties of radiation-induced DNA damage, but also in activation of pro-angiogenic genes, which are crucial for the survival and proliferation of tumors under these adverse conditions.

HIF-1 is a heterodimer composed of α and β subunits, and HIF-1α is regulated in an oxygen-dependent manner at the post-translational level (Semenza and Wang, 1992; Huang *et al.*, 1998; Kallio *et al.*, 1999; Semenza, 2003). In normoxia, HIF-1α is hydroxylated at

its proline residues of the oxygen-dependent degradation (ODD) domain by prolyl hydroxylases (Bruick and McKnight, 2001; Epstein *et al.*, 2001). The modification accelerates the interaction of HIF-1α with the von Hippel–Lindau (VHL) tumor suppressor protein, resulting in the rapid ubiquitination and subsequent degradation of HIF-1α by the 26S proteasome (Cockman *et al.*, 2000; Kamura *et al.*, 2000; Ohh *et al.*, 2000; Tanimoto *et al.*, 2000).

In order to eradicate HIF-1α-expressing hypoxic cells, we have developed TOP3 (TAT-ODD-procaspase-3), a fusion protein with three domains (Figure 1) (Harada *et al.*, 2002, 2005, 2006; Kizaka-Kondoh *et al.*, 2003; Inoue *et al.*, 2004). The PTD is derived from the protein-transduction domain (PTD) of the human immunodeficiency virus type-1 tat protein (Schwarze *et al.*, 1999) and efficiently delivers TOP3 to any tissue *in vivo*. The ODD domain contains a VHL-mediated protein destruction motif of human HIF-1α protein and confers hypoxia-dependent stabilization to TOP3 (Harada *et al.*, 2006). Procaspase-3 is the proenzyme form of human caspase-3 (Fernandes-Alnemri *et al.*, 1994) and confers potential cytocidal activity to TOP3. While TOP3 effectively target hypoxic cells, it does not directly affect the normoxic tumor cells (Harada *et al.*, 2005). On the other hand, IR effectively targets normoxic cells but is less effective to hypoxic cells (Brown, 1999; Vaupel, 2001). Thus, we expect that combination of TOP3 and IR would improve the outcome of antitumor treatment.

Here we demonstrate that the combination of TOP3 and IR efficiently reduced tumor cells with HIF-1 activity induced by both hypoxia and irradiation, leading to long-term suppression of tumor growth and angiogenesis.

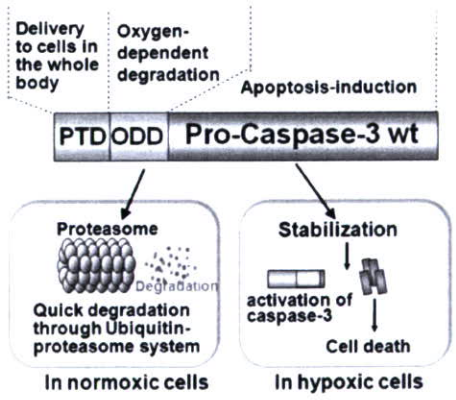

Figure 1 Schematic of structure and domain function of TOP3. TOP3 consists of three domains, which function as drug delivery, oxygen-dependent protein degradation and cell killing. The protein-transduction domain (PTD) enables the fusion protein to diffuse and enter the cell. The stability of TOP3 is regulated by the same mechanism as HIF-1α through the oxygen-dependent degradation (ODD) domain. The procaspase-3 can be activated under hypoxic conditions and induce apoptosis in hypoxic tumor cells.

Results

IR increases HIF-1 activity

Because stabilization of TOP3 is regulated by the same mechanism as HIF-1α (Harada *et al.*, 2006), TOP3 has potential cytosical activity to HIF-1-active cells. Thus, we first examined change in HIF-1 activity in the xenografts during the treatment with IR. HIF-1-driven luciferase activity in HeLa/5HRE-Luc xenografts on the right leg was monitored daily with and without irradiation with 10 Gy. We used this dose because the growth-suppressive effect of TOP3 in combination with 5 Gy IR was less clear, while 20 Gy IR alone was effective enough to remove tumors almost completely and thus the effect of TOP3 was not assessed (data not shown). In the unirradiated animals, HIF-1 activity gradually increased as tumors grew over the observation period (Figure 2a, upper panels and Figure 2b), indicating the total number of hypoxic tumor cells in xenografts increase as tumors grow. With irradiation,

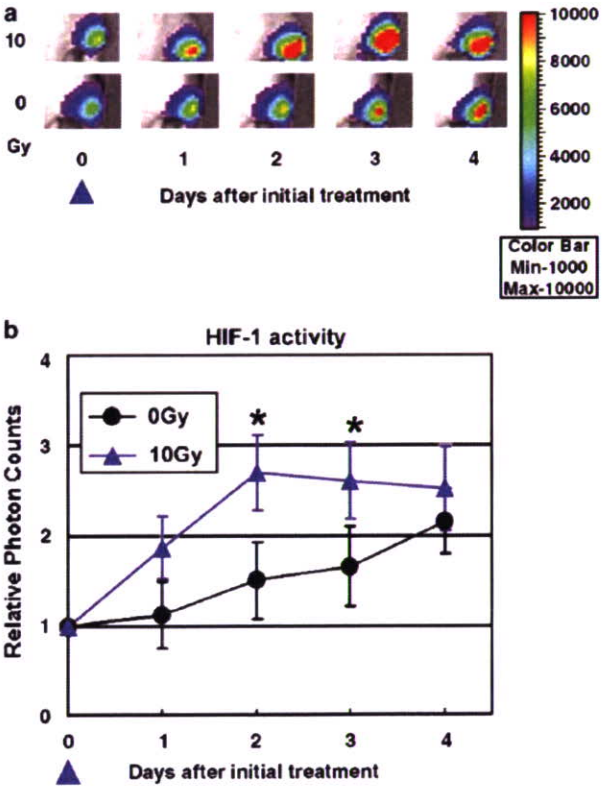

Figure 2 Increase of intratumoral hypoxia-inducible factor-1 (HIF-1) activity by irradiation. Mice ($n=5$ for each group) were transplanted with HeLa/5HRE-Luc cells in the right hind leg. The tumor-bearing mice were treated with local irradiation of xenografts with 0 or 10 Gy on day 0 (blue arrowhead). Change in the intratumoral HIF-1 activity was monitored using bioluminescence (photons/sec) every day with the IVIS photon-counting system. (**a**) A mouse with representative images during the observation period was chosen from the unirradiated (0 Gy) and the 10 Gy-irradiated groups and shown in. (**b**) Photon counts from the xenografts irradiated with 0 and 10 Gy on each day were divided by the corresponding photon counts on day 0 and indicated as relative photon counts. $^*P<0.05$.

HIF-1 activity increased significantly more rapidly for 2 days after irradiation (Figure 2a, lower panels and Figure 2b; $P<0.05$).

Suppression of both hypoxia- and irradiation-induced HIF-1 activities by TOP3

To investigate whether these tumor cells expressing HIF-1 after IR can be target of TOP3, we next examined the antitumor effect of the combination with IR and TOP3. For this purpose, we divided tumor-bearing mice to four groups (buffer, TOP3, IR and TOP3 and IR) and examined effects of monotherapies and the combination therapy on intratumoral HIF-1 activity. When TOP3 was intraperitoneally (i.p.) injected in mice carrying HeLa/5HRE-Luc xenografts on day 0, day 1 and day 2 (Figure 3a), the intratumoral HIF-1 activity was significantly decreased by day 2 (Figure 3a, lower panels and Figure 3b; $P<0.01$). In contrast, HIF-1 activity in buffer-treated HeLa/5HRE-Luc xenografts continuously increased over the observation period (Figure 3a, upper panels and Figure 3b).

Immunohistochemical analysis using an anti-luciferase antibody confirmed that the luciferase protein induced by HIF-1 was localized in the similar region detected by a hypoxia marker, pimonidazole, in untreated xenografts (Figure 3c). In our previous study, the quantitative correlation was demonstrated between the level of HIF-1α expression and the luciferase activity (Harada *et al*., 2005). In the TOP3-treated tumors, HIF-1-induced luciferase and pimonidazole-binding proteins were barely detected (Figure 3c), confirming that TOP3 eliminated HIF-1-active hypoxic cells and reduced the cells reactive with pimonidazole (Harada *et al*., 2005).

In the tumors given IR alone on day 2, HIF-1 activity increased by threefold 2 days after irradiation (Figure 4a, upper panels and Figure 4b). The fold increase of HIF-1 activity of irradiated tumors vs unirradiated tumors from day 2 to day 4 (3.6 vs 2.1, Figures 3b and 4b) was almost identical to the one in Figure 2b (2.5 vs 1.5). When treated with TOP3 for 3 consecutive days from day 0 and irradiated on day 2, the intratumoral HIF-1 activity remained low (approximately threefold of the one on day 0) on day 4 (Figure 4a, lower panels and Figure 4b) and was comparable to the one treated with buffer only on day 4, which was also approximately threefold of the one on day 0 (Figure 3b). This indicated that TOP3 effectively inhibited HIF-1 induced by hypoxia as well as IR.

Suppression of long-term tumor growth by the combination of TOP3 and IR

Next we examined effects of monotherapies and the combination therapy on tumor growth. The growth of HeLa/5HRE-Luc xenografts was significantly but temporarily suppressed by TOP3 alone over a 12-day period (Figure 5a; $P<0.05$ over none). The growth of tumors treated by IR (10 Gy) alone was significantly suppressed starting from 1 week after irradiation (Figure 5a; $P<0.01$ over none). During a 14-day observation period, the combination treatment did not have a significantly

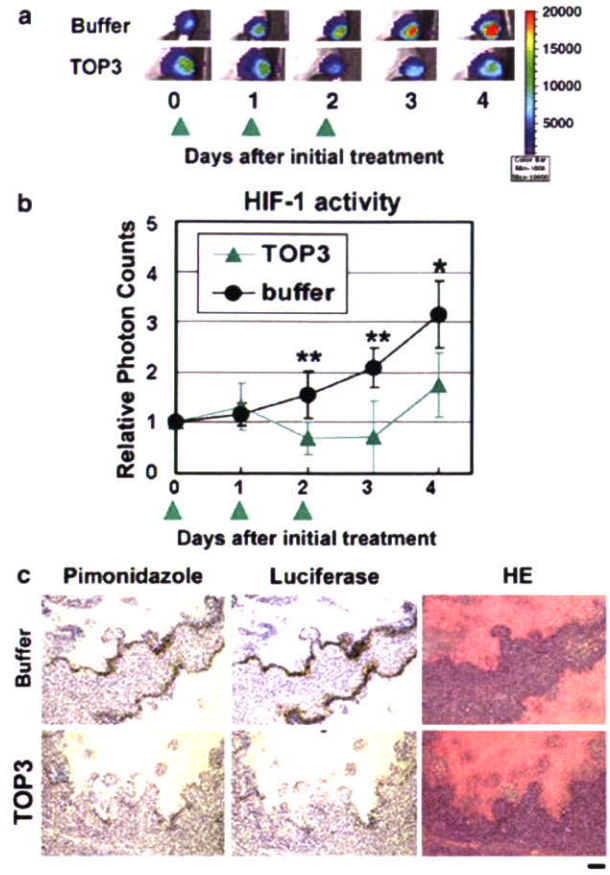

Figure 3 Reduction of hypoxia-induced hypoxia-inducible factor-1 (HIF-1) activity by TAT-ODD-procaspase-3 (TOP3) treatment. Mice ($n=5$ for each group) were transplanted with HeLa/5HRE-Luc cells in the right hind leg. The tumor-bearing mice were treated with local irradiation of xenografts with buffer or TOP3 on day 0, 1 and 2 (green arrowheads). The change in intratumoral HIF-1activity was monitored as described in the legend to Figure 2. (**a**) A mouse with representative images during the observation period was chosen form the control (buffer) and TOP3-treatment (TOP3) groups and shown in. (**b**) Photon counts from the xenografts on each day were divided by the corresponding photon counts on day 0 and indicated as relative photon counts. $*P<0.01$; $**P<0.005$. (**c**) Buffer- or TOP3-treated xenografts were surgically excised on day 2 and used for immunohistochemical analysis with anti-pimonidazole antibody (Pimonidazole), anti-luciferase antibody (Luciferase) and hematoxylin and eosin (HE). Bar = 100 μm.

greater effect than IR alone. However, when the observation was extended to 80 days, the combination treatment was much more effective (Figure 5b). The days required for the tumor volume to increase threefold (tripling time) was 11.1 ± 2.2 days for the buffer-treated animals and 13.6 ± 3.2 days for the TOP3 alone. This small difference due to TOP3 alone was due to the low dose used. This gave us an opportunity to precisely analyse the efficacy of the combination treatment with TOP3 and radiotherapy. The tripling time was 41.6 ± 5.5 days for the IR alone, while that for the combination treatment was 75.7 ± 11.6 days. Thus, a large enhancement was observed for the combination treatment

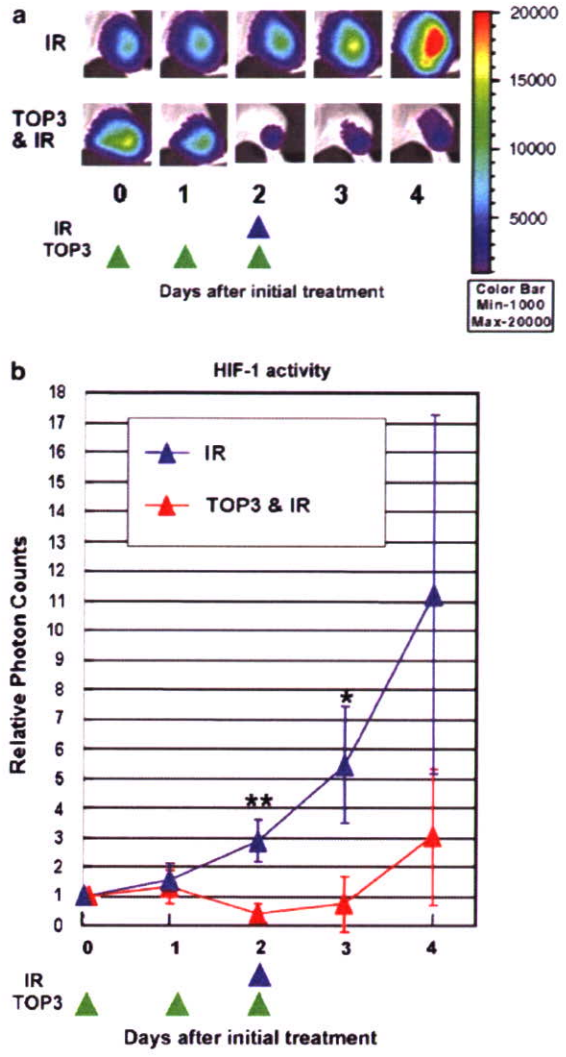

Figure 4 Reduction of the intratumoral hypoxia-inducible factor-1 (HIF-1) activity by TAT-ODD-procaspase-3 (TOP3) and ionizing radiation (IR). Tumor-bearing mice ($n=5$ for each group) with HeLa/5HRE-Luc xenografts in the right hind leg were irradiated with 10 Gy on day 2 (blue arrowhead). Mice of the TOP3 and IR group were additionally treated with TOP3 on day 0, 1 and 2 (green arrowheads). (**a**) A mouse with representative images during the observation period was chosen form the IR-alone group (upper panel) and the TOP3 and IR group (lower panel) and shown in. (**b**) The intratumoral HIF-1 activity was monitored as described in the legend to Figure 2 and presented in the graph. $*P<0.01$; $**P<0.005$.

which delayed tumor growth by 1.8-fold over IR alone. We also tested the combination treatments on CFPAC-1 xenografts and similar results were obtained (Figures 5c and d).

Antiangiogenesis efficacy by TOP3 and IR combination treatment

Although the growth suppression by TOP3 alone was only temporary, the combination treatment resulted in significantly greater effect on the long-term suppression of tumor growth than IR alone (Figure 5). In order to resolve the discrepancy, the histological sections of HeLa/5HRE-Luc xenografts were examined on day 14 for an endothelial marker, CD31. As is clear from Figure 6a, CD31-positive microvessels distributed less in tumors with the combination treatment than those of other groups. Interestingly, TOP3 alone was effective in reducing the microvessels density (Figure 6a). The sections of HeLa/5HRE-Luc xenografts treated as Figure 5a were examined for the microvessel density (the number of microvessels per square millimeter) on day 14 after the initial treatments. The microvessel densities were 31.3 ± 9.5 and $28.5\pm10.0/mm^2$ for the control and IR-treated tumors, respectively which were not statistically different ($P=0.58$) (Figure 6b). In contrast, TOP3 treatment decreased the microvessel density to $17.5\pm3.7/mm^2$ with a good statistical significance ($P<0.001$). Moreover, the combination treatment of TOP3 and IR further reduced the density to $8.5\pm2.0/mm^2$ ($P<0.001$ over TOP3 treatment alone). Although there was a significant difference in the microvessel density between buffer- and TOP3-treated tumors on day 14 (Figures 6a and b), these two exhibited a similar speed of growth thereafter (Figures 5b and d). Immunohistochemical examination revealed that the buffer- and TOP3 alone did not differ in the microvessel density (Figure 6c), indicating anti-angiogenic function of TOP3 was temporary. In contrast, examination of the combination treatment demonstrated long lasting and statistically significant suppression of tumor neovascularizaiton in the tumor (Figure 6d; $P<0.01$ over TOP3 alone).

Discussion

It has long been recognized that the tumor hypoxia is a critical limit to radiotherapy. Various radiosensitizers have been developed in the past, which were designed to sensitize hypoxic tumor cells to radiation. However, their clinical use was hampered because of their neurotoxicity and low efficacy (Rowinsky, 1999; Zackrisson *et al*., 2003; Overgaard *et al*., 2005; Rischin *et al*., 2005). Recently, Sobhanifar *et al*. (2005) examined human tumor biopsies and human cancer xenografts with expression of HIF-1α and distribution of a chemical hypoxia marker, pimonidazole, which become reactive at less than 10 mm Hg oxygen tension. They found that expression of HIF-1α was reduced in the pimonidazole-positive regions, which are the target of the most of hypoxic cytotoxins. This suggests that these hypoxic cytotoxins are less effective in HIF-1-active hypoxic cells and may explain in part their low efficiency *in vivo*. HIF-1-active tumor cells have recently become a central issue for not only radiotherapy, but also for general tumor therapy since HIF-1 is now known to activate a variety of genes involved in anti-apoptosis and angiogenesis (Semenza, 2003).